DOKUZ EYLÜL UNIVERSITY
GRADUATE SCHOOL OF NATURAL AND APPLIED SCIENCES

NUMERICAL MODELLING OF PHASE CHANGE MATERIAL INTEGRATED METAL HYDRIDE HYDROGEN STORAGE TANK

by
Tacettin DİŞLİ

December, 2023
İZMİR

NUMERICAL MODELLING OF PHASE CHANGE MATERIAL INTEGRATED METAL HYDRIDE HYDROGEN STORAGE TANK

A Thesis Submitted to the
Graduate School of Natural and Applied Sciences of Dokuz Eylül University
In Partial Fulfillment of the Requirements for Master of Science in
Department of Mechanical Engineering, Thermodynamics Program

by
Tacettin DİŞLİ

December, 2023
İZMİR

M.Sc THESIS EXAMINATION RESULT FORM

We have read the thesis entitled **"NUMERICAL MODELLING OF PHASE CHANGE MATERIAL INTEGRATED METAL HYDRIDE HYDROGEN STORAGE TANK"** completed by **TACETTİN DİŞLİ** under supervision of **ASSOC.PROF.DR. MEHMET AKİF EZAN** and we certify that in our opinion it is fully adequate, in scope and in quality, as a thesis for the degree of Master of Science.

....

Assoc.Prof.Dr. Mehmet Akif EZAN

Supervisor

....

Prof. Dr. Can Özgür ÇOLPAN

Jury Member

....

Prof. Dr. Önder KIZILKAN

Jury Member

Prof. Dr. Okan FISTIKOĞLU

Director

Graduate School of Natural and Applied Sciences

ACKNOWLEDGMENT

The author wishes to express deep gratitude to supervisor Assoc. Dr. Mehmet Akif EZAN for his invaluable supervision, advice, encouragement, support, and insight throughout the research process.

The author is eternally grateful to his TUBITAK Principal Investigator who contributed to enriching the thesis with his valuable comment, Prof. Dr. Can Özgür ÇOLPAN.

The author wishes to express his special thanks to his dear friends Sera Ayten ÇETİNKAYA, Rahime ALSANĞUR, Eda KUMCUOĞLU, Aykut KORKMAZ, Cemil KUZU and Okan GÖK for their valuable contributions.

The author thanks to The Scientific and Technological Research Council of Turkey TUBITAK 2535 (Grant number: 220N405) Project.

The author gratefully thanks to his family for their invaluable support in his entire life.

Tacettin DİŞLİ

NUMERICAL MODELLING OF PHASE CHANGE MATERIAL INTEGRATED METAL HYDRIDE HYDROGEN STORAGE TANK

ABSTRACT

In this study, numerical investigations on the performance of the charging process of a metal hydride-based hydrogen storage tank are presented. Three scenarios were developed to examine the absorption performance and compare the effectiveness of the proposed thermal management alternatives. In Scenario-1, the metal hydride (MH) tank is cooled by convective heat transfer, i.e., external convection, on the side surface of the tank. In scenario-2, phase change material (PCM) is wrapped around the MH tank to investigate passive thermal management. A hybrid approach, Scenario-3 includes the PCM layer and an internal heat sink. In this scenario, the heat transfer fluid (HTF) inside the tube is activated depending on the temperature inside the MH tank. A 2D axisymmetric numerical code was developed using the finite volume approach in MATLAB software. In parametric study, (i) charge pressure, (ii) external convective heat transfer coefficient, (iii) PCM thickness, (iv) latent heat of PCM, (v) PCM melting temperature (vi) HTF temperature (vii) convection coefficient of HTF (viii) porosity parameters are considered and a total of 379 parametric analyzes were performed. Time-dependent variations of hybrid bed temperature and weight ratio were evaluated for each scenario. As a result, it has been observed that storage performance is strongly dependent on the transport coefficient at ambient conditions. While the storage criteria were determined according to different thermal management strategies, PCM thickness and latent heat of fusion showed higher storage performance than the external convection coefficient at the same charge pressure.

Keywords: Cooling channel, hydrogen storage, mathematical model, metal hydride, pcm

FAZ DEĞİŞİM MALZEMESİ ENTEGRELİ METAL HİDRİT HİDROJEN DEPOLAMA TANKININ SAYISAL MODELLENMESİ

ÖZ

Bu çalışma, metal hidrit hidrojen depolama tankında absorpsiyon prosesinin performansına ilişkin sayısal araştırmaları içermektedir. Absorpsiyon performansını incelemek ve farklı termal yönetim sistemlerinin etkinliğini karşılaştırmak için üç farklı senaryo geliştirilmiştir. Senaryo-1, metal hidrit tankının lateral yüzeylerden zorlanmış taşınım ile soğutulmasını incelemektedir. Senaryo-2'de pasif termal yönetim sistemini incelemek için tankın etrafına faz değişim malzemesi (FDM) sarılmıştır. Hibrit termal yönetim sistemi olan Senaryo-3'de, FDM katmanı ve merkeze konumlandırılmış soğutma kanalı ile absorpsiyon performansının incelenmesi amaçlanmıştır. Bu senaryoda, MH tankının sıcaklığına bağlı olarak soğutma kanalı içindeki ısı transferi akışkanı (ITA) aktifleşmektedir. Sonlu farklar yöntemi kullanılarak, MATLAB ortamında 2B eksenel simetrik sayısal kod geliştirilmiştir. Yapılan parametrik çalışmalarda, (i) şarj basıncı (ii) taşınım katsayısı (iii) FDM kalınlığı (iv) FDM'nin gizli ısısı (v) FDM erime sıcaklığı (vi) ısı transferi akışkanı sıcaklığı (vii) ısı transferi akışkanının taşınım katsayısı (viii) hidrit yatak gözenekliliği gibi kritik parametreler belirlenerek 379 adet parametrik analiz gerçekleştirilmiştir. Hidrit yatak sıcaklığı ve ağırlık oranının zamana bağlı değişimleri her bir senaryo için değerlendirilmiştir. Sonuç olarak, taşınım katsayısının depolama performansı açısından oldukça etkili bir parametre olduğu gözlemlenmiştir. Depolama kriterleri farklı termal yönetim stratejilerine göre belirlenirken, FDM kalınlığı ve gizli ısı paremetrelerinin aynı şarj basıncında yan yüzeylere uygulanan taşınım katsayısından daha yüksek depolama performansı gösterdiği gözlemlenmiştir.

Anahtar kelimeler: FDM, hidrojen depolama, matematiksel model, metal hidrit, soğutma kanalı

CONTENTS

Page

LIST OF FIGURES

Page

LIST OF TABLES

Page

CHAPTER ONE
INTRODUCTION

1.1 Introduction

Today, population growth increases the demand for energy. Efforts persist in mitigating the detrimental impacts of climate change and greenhouse gas emissions through technological advancements. As a result, there is a tendency towards alternative energy sources due to the negative effect of fossil fuels. Some countries, such as Japan, have started to work towards the transition to the hydrogen age by 2030 (Dincer, 2020). In the Paris Agreement created in 2015, which Turkey signed, it was stated that the use of energy resources such as coal and oil, caused by global warming, would gradually decrease, and that renewable energy resources would be used instead. In addition, all states that signed the Paris Agreement are taking steps towards the zero-carbon target.

Turkey possesses the capability to both generate hydrogen, a substance gaining prevalence in various global sectors, and emerge as a technology innovator in the short, medium, and long term. Recognizing this potential, the report outlines the requirements for advancing hydrogen technologies in Turkey and proposes technological and supportive solutions. Also, Turkish government states that electrolyzer installed power capacity will increase to 2 GW by 2030, 5 GW 2035 and 70 GW by 2053. There are also some studies on hydrogen storage studies. Turkey Ministery of Energy and Natural Resources has announced a road map for hydrogen storage with complex hydrides until 2030. Hydrogen storage systems, which are planned to be used in ground vehicles, marine vehicles and aviation applications until 2040, are being designed (Yilmaz et al., 2023).

Hydrogen energy is seen as a serious alternative to meet the world's energy needs. Hydrogen is a naturally occurring and very common element and only water vapor is formed during combustion. This indicates that the use of hydrogen energy is a much more friendly energy source for atmospheric emissions. In addition, hydrogen energy is a flexible energy source and can provide energy for different types of vehicles, homes and industrial enterprises using a suitable storage system. Hydrogen also makes it possible to create an energy ecosystem based on long-term energy sources. While energy sources such as oil, natural gas and coal are limited and depleted over time, hydrogen energy can be produced and used on an ongoing basis. In addition, hydrogen energy is a naturally produced energy source, such as wind, solar, hydro, and other renewable energy sources.

As a result, hydrogen energy is accepted as an important alternative to meet energy needs worldwide. Due to the depletion of limited energy resources and the need to reduce atmospheric emissions, hydrogen energy will continue to meet a significant amount of the world's energy needs in the future.

The hydrogen energy system's production and storage of hydrogen are vital elements. Hydrogen can be produced in a variety of ways, including biomass gasification, water electrolysis, and steam methane reformation. The most popular technique for producing hydrogen is steam methane reformation, which involves mixing natural gas with hot steam to create both hydrogen and carbon dioxide. On the other hand, water electrolysis uses electricity to divide water into hydrogen and oxygen. Through a series of chemical reactions, organic matter is transformed into hydrogen during the process of biomass gasification.

After it is generated, hydrogen needs to be stored for usage of customer. A solid, a liquid, or a gaseous form of hydrogen can all be stored. Gaseous hydrogen is stored most frequently, especially in high-pressure tanks. Within the scope of the thesis, hydrogen storage in simple metal hydrides will be examined.

Metal hydrides are materials that can store hydrogen in a solid phase, making them a promising method for hydrogen storage instead of compressed or liquid methods.

CHAPTER TWO

BACKGROUND AND LITERATURE SURVEY

2.1 Hydrogen Storage Methods

Hydrogen has the huge potential to play a vital role in the transformation to a zero-carbon energy system. Nevertheless, the usage of hydrogen as a fuel is quite challenging due to its filling criteria. Hydrogen has a low energy density per unit volume compared to fossil fuels. In order to have the same effect as fossil fuels, more expensive, heavy storage tanks must be used. Current studies are aimed at determining the feasibility studies of hydrogen storage (Barthelemy, Weber & Barbier, 2017).

There are several ways to store hydrogen, by using compressed tank, liquid hydrogen (cryo-tank) storage, and solid-phase storage. Each of these storage methods has its own pros and cons, and researchers are working to develop new storage methods that can improve the efficiency, safety, and low cost of hydrogen storage (Zhou, 2005). Extended hydrogen storage methods according to the standards are shown in Figure 2.1 (Montenegro, Sanjuan & Carmona, 2019).

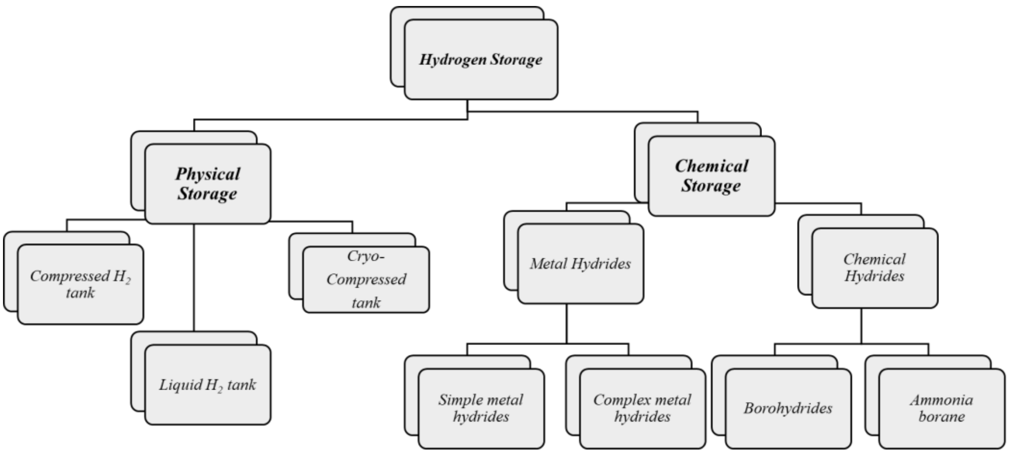

Figure 2.1 Hydrogen Storage Methods (adapted from Montenegro et al., 2019)

2.1.1 Physical Storage

Various physical storage methods have been developed to overcome some hydrogen storage criteria problems and make hydrogen as usable energy carrier.

The utilization of compressed hydrogen gas is one of the most popular physical storage techniques. This technique containing compressing hydrogen to a high static pressure of up to 700 bar and storing it in high-pressure containers made of durable and light-weight materials like carbon fiber or metal alloys (Barthelemy et al., 2017). Fuel cell vehicles can use compressed hydrogen gas because of its high energy density, but doing so necessitates a sizable storage facility and high-pressure filling infrastructure (Nitta, Himanen & Mikkola, 2008).

Another method, hydrogen can be stored in cryogenic hydrogen containers. Hydrogen is cooled down to 21 K and stored in cryogenic tanks in open systems. The challenges of this method are energy-efficiency and cost of the cryogenic tank. In addition thermal insulation should be provided for efficient storage (Züttel, 2004).

2.1.2 Chemical Storage

Chemically, the hydrogen storage method is basically divided into two parts as simple and complex metal hydride. For this method, storage is provided by the formation of bonds of hydrogen with group AB compounds. Heat transfer and reaction kinetic mechanisms strongly influence charge/discharge processes.

Simple metal hydride compounds are made of a combination of one metal and hydrogen (MgH_2, NaH, TiH_2). They have relatively low storage capacities, and they can generally store 10% of their weight. In addition, they have low cost and by applying heat transfer mechanisms, charge/discharge processes can be managed quickly compared to complex hydrides (Mohamed, 2019).

Complex metal hydrides, on the other hand, are formed by the combination of multiple metal and/or non-metal compounds and hydrogen ($NaAlH_4$, $LiBH_4$). Storage capacity is higher (10-18%) than simple metal hydrides. On the other hand, the absorption or desorption processes are quite slow compared to simple hydrides. In addition, they are more costly and have higher activation energy.

The volumetric density and weight ratio relationship of some metal hydride types is described in Figure 2.2. According to the storage systems classified according to the utility energy use report of the energy department, metal hydrides are promising for the future due to their high energy storage capacity compared to liquid hydrogen storage and storage in compressed tanks (Møller et al., 2017).

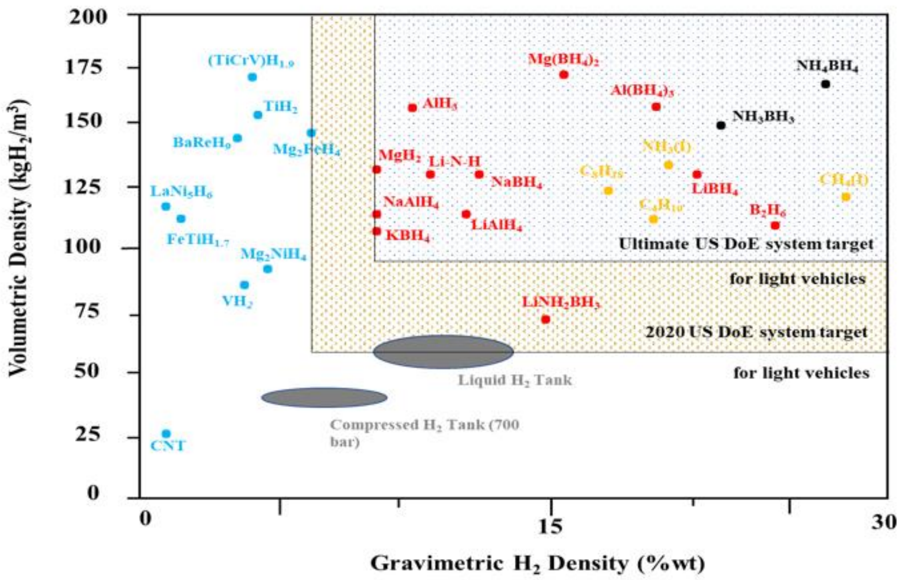

Figure 2.2 Volumetric Density and Weight Ratio for Hydrogen Storage (adapted by Møller et al., 2017).

2.2 Nature of Metal Hydrides

Hydride compounds provide storage by taking advantage of the chemical properties of hydrogen. It tends to bond to the metal during the filling of hydrogen in the metal hydride tank (absorption). Heat is produced as a result of this exothermic process. The reverse process occurs when hydrogen is released from the hydride reactor (desorption), and the reaction absorbs heat. The general sorption scheme used in metal hydride system is shown in Figure 2.3 (Muthukumar et al., 2018),

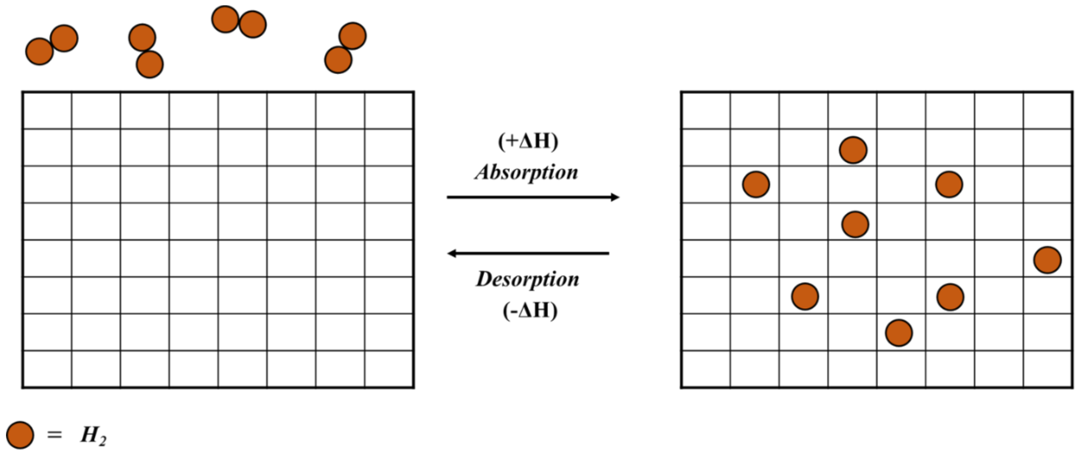

Figure 2.3 Metal Hydride Sorption Scheme (Muthukumar et al., 2018)

The chemical reaction, absorption and desorption processes of the metal hydride bed are defined in Equation 2.1. Since the absorption process is exothermic, the heat must be removed from the system in order to achieve hydritization. In the desorption process, the hydride bed needs additional heat energy to dehydritization. The choice of hydride material gains considerable importance in terms of weight ratio and releasing heat energy, which will be explained in the next chapter.

$$M + \frac{x}{2}H_2 \leftrightarrow MH_x \tag{2.1}$$

where M represents the metal.

2.3 Hydride Material Selection

Material selection is a vital factor determining the performance of hydrogen storage systems. Many factors are considered in material selection, such as hydrogen holding capacity, kinetic properties, thermal stability and non-toxicity. One of these factors is hydride types. The most commonly used materials are AB, AB_2 and AB_5 intermetallic alloys (Afzal et al., 2017).

2.3.1 AB Intermetallic Compounds

A class of compounds known as intermetallic compounds, or AB intermetallic compounds, typically contain two different metallic elements in a stoichiometric ratio. These substances have distinct mechanical, electrical, and magnetic properties, as well as a clearly defined crystal structure. It is possible to form a distinct compound with particular properties because the A and B elements in the compound typically have different properties. The most prominent example of these metallic compounds is the TiFe alloy. Instead of Fe, Ni or Mn can also form compounds with Ti.

2.3.2 AB_2 Intermetallic Compounds

AB_2 family has a wide range that mixes with A and B in a certain ratio to form the hydride material. Element A is usually composed of Zr and Ti. B element, on the other hand, consists of V, Cr and Mn depending on its chemical bonding capacity.

Pressure-concentration-temperature (PCT) curve of basic AB_2 compounds proves that they work at low equilibrium pressure (2-12 bar) and temperature (0-100 °C). It is less costly than AB and AB_5 compounds. The PCT curve for typical AB_2 metal is presented in Figure 2.4,

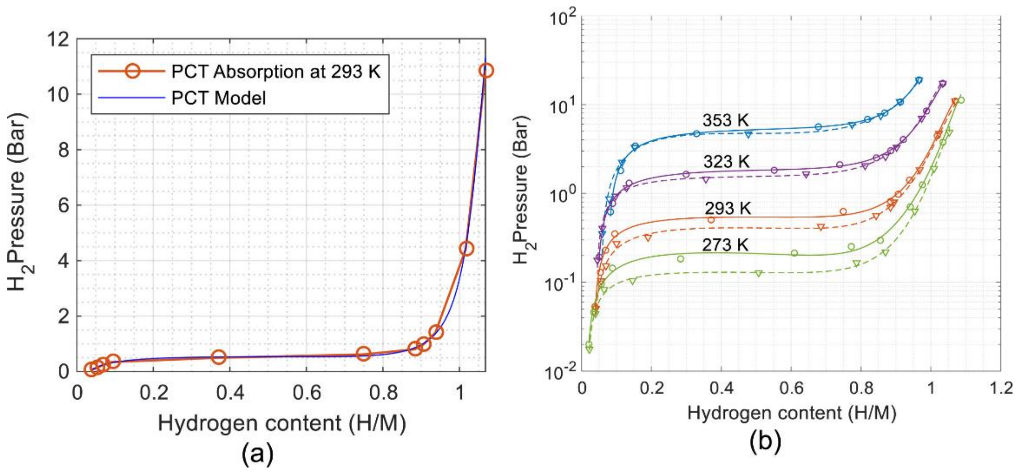

Figure 2.4 PCT Curves for typical AB_2 ($AB_{1.95}$) Compound (Hariyadi et al., 2022)

2.3.3 AB_5 Intermetallic Compounds

AB_5 type hydrogen storage alloys generally consist of the main element A and the alloy of transition metals such as Ni, Co, Mn. It has a large family of members such as AB_2 type intermetallic compounds.

$LaNi_5$ is the most used intermetallic compound in modeling and experimental applications. It is chemically easy to obtain compared to other types. In terms of weight fraction, it does not exceed its storage capacity of 1.3%. For this reason, it is called a low temperature hydride. The chemical properties for the most commonly used metal hydride types in the literature are defined in Table 2.1 (Cetinkaya et al., 2022).

Table 2.1 Chemical Properties of Hydride Types (Cetinkaya et al., 2022)

Hydride Types	**Working Temperature Range (T_L-T_H) °C**	**-ΔH Enthalpy (kJ/mol-H_2)**	**ΔS Entropy (kJ/molH_2K)**
$Ti_{0.9}Zr_{0.1}Mn_{1.4}Cr_{0.35}V_{0.2}Fe_{0.05}$	25-100	25.89	106.9
$LaNi_5$	25-200	31.80	110
$TiFe_{0.9}Mn_{0.1}$	0-100	29.70	107.7
$LaNi_{4.7}Sn_{0.3}$	25-80	36.51	112.6
$MmNi_{4.15}Fe_{0.85}$	25-200	25	105.4
$TiCr_{1.5}Mn_{0.25}Fe_{0.25}$	10-165	19.32	101.6
$LaNi_{4.7}Al_{0.3}$	20-80	29.21	98
$LaNi_{4.6}Al_{0.4}$	20-80	34.04	108
$TiCr_{1.8}$	0-100	20.2	111
$Ti_{0.98}Zr_{0.02}V_{0.43}$	0-100	27.4	112

2.4 Pressure Concentration Temperature (PCT) Curve

The PCT curve needs to be explained in order to comprehend the reaction continuity, hydride weight ratio, and temperature-pressure relationship in the sorption process of metal hydrides.

In the PCT curve shown in Figure 2.5, the relationship of hydrogen capacity, equivalent pressure and temperature is discussed. The plateau region is characterized as the study region for the hydride type under consideration. The equivalent pressure determined in the Van't Hoff equation calculates the pressure range in the plateau region. Van't Hoff equation will be given in the mathematical modeling chapter. In addition, the equivalent equilibrium pressure can be found for each wt% by calculating the PCT curve with empirical relations. In the absorption process, the continuity of the reaction continues depending on the comparison between the charge pressure and the equivalent pressure. For the reaction to continue, the operation pressure must always be greater than the equilibrium pressure. In the desorption process, the equilibrium pressure should be greater than the vacuum pressure.

The hysteresis factor can be defined as the loss of the thermodynamic cycle as a result of the absorption and desorption processes. The hysteresis length is desired to be short for longer life and performance in practical uses. This length varies depending on the metal hydride type and operating temperature (Sandrock, 1999).

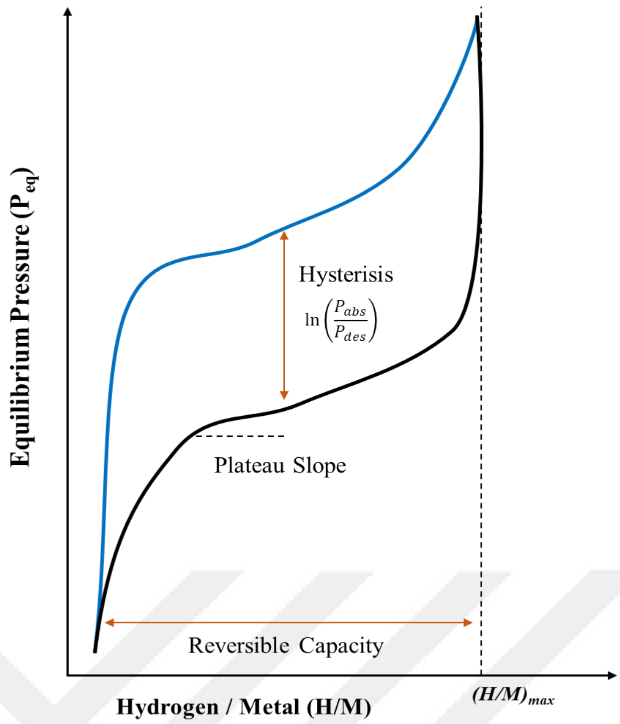

Figure 2.5 Definition of PCT Curve Components (modified from Sandrock, 1999)

2.5 Literature Survey

In this section, the studies in the metal hydride reactor are examined in two main parts. The effects of the approaches used in mathematical modeling and thermal management strategies on storage and tank temperature have been observed.

2.5.1 Studies on mathematical modeling of metal hydride reactor

The mathematical modeling of the metal hydride container is based on simultaneous analysis of heat and mass transfer. There are numerous papers in the literature examining the absorption process of the metal hydride tank experimentally and numerically. Jemni and Nasrallah (Jemni, 1995) created a 2D mathematical model. Unsteady constructed the heat and mass transfer equations for the notation control domain using the finite difference method. They defined a discontinuous porous media for the hydride (solid) and hydrogen (gas) domains. In addition, they assumed that positional pressure change of the hydrogen gas can be neglected. They stated that the effect of parameters such as operating pressure and inlet temperature on storage is very important. On the other hand, they showed that the term heat transport by convection can be neglected. Aldas et al. (Aldas et al., 2002) created a 3D mathematical model. The energy equation and heat-mass transfer equations were calculated with a fully implicit scheme for the absorption process. They examined active thermal management with the cooling channel and identified some findings. According to the findings, hydride tank temperature is a quite relevant function for hydritization. In addition, surprisingly, the overall hydride formation is not a function of the cooling fluid velocity ty, even if the velocity of the cooling fluid reduces the temperature profile of the hydride bed. Nakagawa et al. (Nakagawa, 2000) developed a mathematical model using the 2D axisymmetric coordinate system. They analyzed the model they were considering numerically with the finite element method. They integrated the effects of permeability into the chemical equation. Furthermore, they designed a system in which the outer domain of the hydride bed is strongly managed with a cooling and heating system for absorption and desorption processes. They stated that the convection coefficient had positive effects on the hydritization formation. Moreover, using some empirical formulations in the literature, they specified the time-dependent weight ratio for certain situations. Busqué et al. (Busqué, Torres, Grau, Roda & Husar, 2018) investigated the sorption process in a metal hydride tank numerically and experimentally. They numerically developed the 2D axisymmetric model using COMSOL software. In addition, they compared the temperature-time and pressure-time curves experimentally and numerically. While constructing the model, the solid and gaseous hydrogen temperatures were assumed to be the same. They neglected the volumetric expansion during the sorption process. They noted the positive sorption effects of porosity, reaction enthalpy and external convection coefficient. Tong et al. (Tong, Xiao, Yang, Bénard, Chahine, 2019) modeled metal hydride tanks in 3D and 6 different cases in the COMSOL software. Different types of heat exchanger and coil designs were compared with the plain hydride bed to ensure the thermal management of the tank. While constructing the mathematical model, they neglected the effects of the reactor walls on the hydride domain. Unlike other studies, they also considered the momentum equation. They calculated parameters such as hydrogen absorption capacity and mean temperature for 5 different heat exchanger designs. They found that the performance of the flat plain hydride mattress was inefficient compared to different heat exchanger designs. In addition, for the single coiled-tube heat exchanger, they reduced the 3D model to 2D. Askri et al. (Askri, Jemni & Nasrallah, 2004) mathematically modeled the metal hydride tank in 2D as a transient state. The constructed model was solved numerically using the finite volume method used by PHOENICS. In the modeling, they neglected the viscous separations and accepted the term dispersion as diffusive flux. They calculated the position-dependent hydride density and operating pressure for specific time intervals. They also determined velocity distribution inside the hydride bed domain. They compared the expansion volume with the inner domain of the metal hydride tank and noted that the velocity distributions in the inner domain had little effect on the sorption process. Bao et al. (Bao, Yang, Wu, Cao & Zhang, 2013) constructed a 1D system consisting of compact high-temperature hydride discs (MgH_2) and heat transfer pipe using COMSOL software. They defined the continuity and Navier-Stokes equations for the void zone through which hydrogen enters. They determined the gas velocity, gas pressure and temperature distributions for different time periods. They performed parametric analysis for the boost pressure. They stated that when the inlet velocity of the gas increases, the absorption process sharply accelerates. An overall assessment of the literature is presented in Table 2.2.

Table 2.2 Overall Assessment of Literature Survey

Study	**Year**	**Dimension**	**Method/Software**	**Assumptions/ Reductions**
(Jemni & Nasrallah 1995)	1995	2D	Finite difference	Positional pressure changes of the gas neglected
(Nakagawa et al., 2000)	2000	2D	Finite element	Capability of permeability factor
(Aldas et al., 2002)	2002	3D	Fully implicit scheme	N/A
(Askri, 2004)	2004	2D	PHOENICS Code	Viscous effects of hydride bed neglected
(Bao et al., 2013)	2013	1D	COMSOL	Definition of Navier Stokes equation for void zone
(Busqué et al., 2018)	2018	2D	COMSOL	Solid and gas temperature are the same
(Tong et al., 2019)	2019	3D	COMSOL	The effects of the reactor walls on hydride bed neglected

2.5.2 Studies on thermal management systems of metal hydride reactor

Exothermic and endothermic chemical reactions during hydritization and dehydration processes cause temperature variations inside the hydride bed. The kinetic reactions within the metal hydride significantly depend on the temperature; that is, the flow rate of the charged or discharged hydrogen is highly affected by the thermal management system of the tank. Therefore, it is important for tank performance that a suitable thermal management technique be used during charge/discharge in metal hydride tanks. Various thermal management techniques could be applied to the tank, either active or passive, to control the reaction rate (Cetinkaya et al., 2022). Passive thermal management are methods that use natural convection such as using fins (Askri, Ben Salah, Jemni & Nasrallah, 2009; Gupta & Sharma, 2021), PCMs (Mghari, Huot & Xiao 2019; Facci, Lauricella, Succi, Villani & Falcucci, 2021), metal foams (Bai, Yang, Tang, Dai, S.Yang, 2022), flakes (Madaria & Kumar, 2016), or high thermal conductivity materials (Suda, Komazaki & Kobayashi, 1983). Unlike passive thermal management, active thermal management employs forced convection to increase heat transfer using heat transfer fluid tubes (Karmakar, Mallik, Gupta & Sharma, 2021), water jacket (Gupta & Sharma, 2021), or air flow by fan (Borzenko & Eronin, 2016). Askri et al. (Askri et al., 2009) mathematically modeled the metal hydride tank with internal and external fins. They reported that the MH tank with internal fin filled faster than the other thermal management methods. They stated that the storage time was reduced by 80% when the fin was added to the MH reactor. Darzi et al. (Darzi, Afrouzi, Moshfegh & Farhadi, 2016) developed a 2D axisymmetric model to examine the performance of a PCM-integrated $LaNi_5$ based metal-hydride hydrogen storage container for absorption and desorption processes. They performed the effects of parameters such as weight ratio and porosity on the absorption process. In addition, they observed that the application of metal foam into the PCM had a positive effect on the PCM liquid fraction and charging time. Alqahtani et al. (Alqahtani, Mellouli, Bamasag, Askri & Phelan, 2020) studied the absorption and desorption performance of metal hydride according to the position of the PCM. In the case with PCM wrapped inside and around the tank, 81% more effective storage was achieved compared to the PCM wrapped just outside the tank. El Mghari et al. (El Mghari, Huot, Tong & Xiao,

2020) investigated the PCM and hydride reactor numerically for the absorption and desorption processes using the COMSOL software. They reported some results on the storage time of the thermal conductivity coefficient of PCM. They observed that when they increased the thermal conductivity coefficient from 0.24 to 2.4 W/mK, the storage time decreased, and the sorption process could be more performance by choosing a PCM at the appropriate melting temperature. Hassan et al. studied the filling performance of multilayer PCM for the absorption process in a metal hydride tank. They performed a parametric study to investigate the effect of the thermal conductivity of PCM on this storage performance. As a result, they stated that the storage time was reduced by 78% in the use of four layer PCM when compared to the reference study and the other cases (Hassan et al., 2023). Kumar et al. (Kumar, Raju, Muthukumar & Selvan, 2019) experimentally investigated a metal hydride tank based on $LaNi_{4.7} Al_{0.3}$ embedded in a cooling tube. Various parametric analyzes were performed by changing the temperature of the heat transfer fluid and the charging pressure. 402.66 g of hydrogen were found to be absorbed in 1908 seconds at a low charging pressure of 2 bar with HTF at 30 °C and 30 L/min flow rate. 413,586 grams of hydrogen was absorbed at 5 bar at the supply pressure and decreased by 466 s (25%) compared to a full charge at 2 bar. On the other hand, 424,867 grams of hydrogen was absorbed when the supply pressure was 10 bar and decreased by 655 s (37%) compared to a full charge at 2 bar. Busque et al. (Busqué et al., 2018) developed an experimental setup and a 2D axisymmetric model to perform the desorption process. They used a heater fan as thermal management and examined the effects of parameters such as convection coefficient, porosity, and reaction enthalpy. Chung et al. (Chung, Chen, P. Chen, Chang, 2015) performed CFD analysis to examine the effect of the fin usage on the absorption time and heat transfer rate in an internal fin attached metal hydride reactor. They compared three different cases, a thin fin, a medium fin, and a metal hydride reactor without a fin. As a result, it is stated that the case with thin fins is charged faster and the temperature rise is less. Various passive thermal management configurations used in the literature are shown in Figure 2.6.

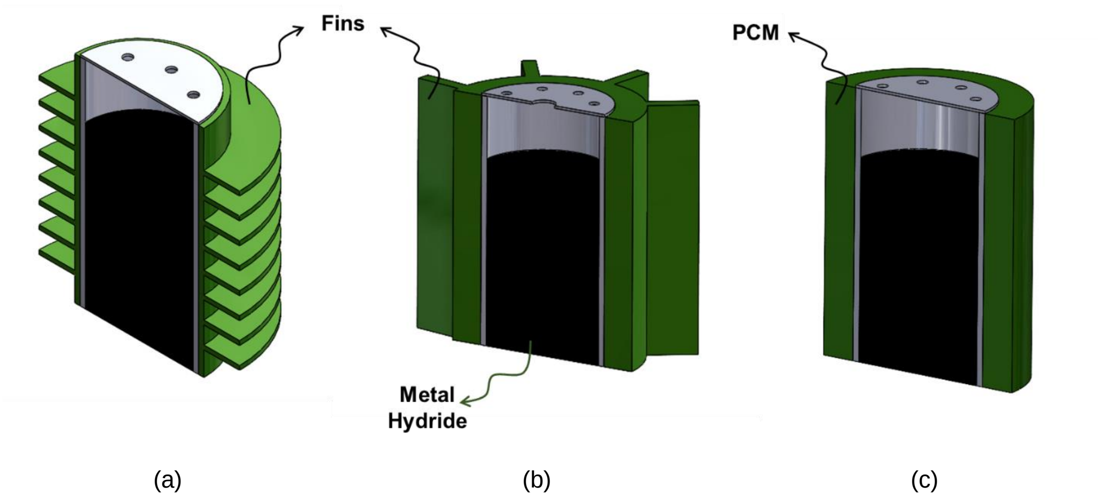

Figure 2.6 Passive Thermal Management Methods with (a) Horizontal Fins (modified from (Askri et al., 2009)), (b) Longitudinal Fins (Modified from (modified from Bai et al., 2022)) and (c) Phase Change Material

The literature also contains studies of hydride thermal management methods. Miled et al. (Miled, Melluoli, Maad & Askri, 2017) developed a 2D mathematical model with a PCM and a cooling channel. They examined PCM melting fraction, thermal conductivity of PCM, and heat transfer coefficient at specific time intervals. In simulations, they have assumed constant PCM thickness and convective heat transfer coefficient for the heat transfer fluid inside the channel. The internal cooling was active throughout the charging process. Mellouli et al. (Mellouli, Askri, Dha 2010) investigated the effects of fin and heat exchanger on the storage time and heat transfer mechanism in a $LaNi_5$ based metal hydride hydrogen storage tank. They performed parametric studies by proposing different heat exchangers and fin designs. They stated that the metal hydride storage tank with fin and exchanger has a 66% better heat transfer rate and provides 90% faster storage than the plain structure. Tong et al. (Tong, Xiao, Yang, et al., 2019) analyzed the fin and cooling channel combinations using COMSOL software to examine the system performance for the absorption and desorption reactions of the metal hydride tank. They reported that the storage capacity for the same case is maximum in 380 seconds, and it has higher performance compared to other cases. Considering all the outputs, they did not study the PCM effect and the controlled opening and closing mechanism of the cooling channel due to the increase in hydride reactor temperature. In addition, the flow inside the cooling channel was active throughout the simulations. Gupta and Sharma (Gupta & Sharma, 2021) numerically created the internal copper fin and water cooling system using the finite volume method in ANSYS CFX to examine the absorption and desorption processes of the $LaNi_5$ based hydride bed. They examined the charge/discharge times as a result of parametric analyzes such as the number of fins and their length. As a result, it was stated that the use of the fin reduced the hydride bed temperature by 22.3 °C during charging and 6.8 °C during discharge. A summary of the thermal management strategies used in MH tanks is given in Table 2.3. Also, different active and hybrid thermal management configurations found in the literature are shown in Figure 2.7.

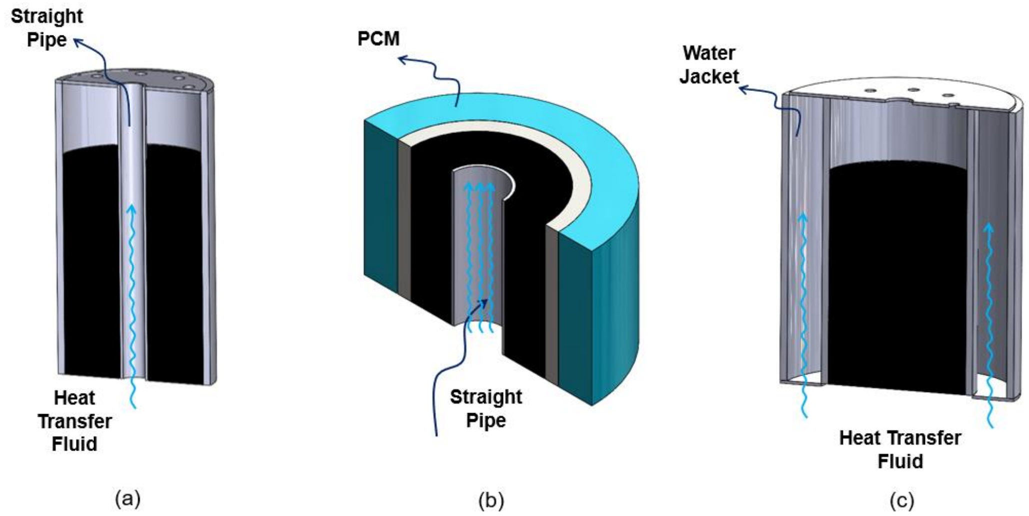

Figure 2.7 Active and Hybrid Thermal Management Methods with (a) Using Straight Pipe (modified from (Tong et al., 2019)) (b) PCM and Straight Pipe Configurations (modified from (El Mghari et al., 2019)) (c) Using Water Jacket

Table 2.3 Reviews on Thermal Management systems used in the MH Hydrogen Storage Tank

Study	Year	Experimental or Numerical	Thermal Management System
Askri et al.	2009	Numerical	Passive (Internal fin, external fin)
Melloulli et al.	2010	Numerical	Active (Fin, heat exchanger)
Chung et al.	2015	Numerical	Passive (Internal fin)
Darzi et al.	2016	Numerical	Passive (PCM)
Miled et al.	2017	Numerical	Passive (PCM, internal fin)
Busque et al.	2018	Experimental	Active (Heater fan)
Kumar et al.	2019	Experimental	Passive (Internal fin)
Mghari et al.	2019	Numerical	Passive (PCM)
Tong et al.	2019	Numerical	Hybrid (Internal and external fin, straight pipe heat exchanger)
Alqathani et al.	2020	Numerical	Passive (PCM)
Gupta and Sharma	2021	Numerical	Active (Fin, cylindrical cooling channel)
Hassan et al.	2023	Numerical	Passive (PCM)

2.6 Motivation

This thesis focuses on the analysis and modeling of the PCM integrated $LaNi_5$ based metal hydride tank for the absorption reaction. The primary motivation of this thesis as;

- The 2D mathematical model of metal hydride hydrogen storage tank was developed in the MATLAB environment. The developed model verified by the study in the literature. Outputs such as hydride bed temperature and weight ratio were performed by examining different thermal management systems such as cooling channel and forced convection, apart from PCM. The primary motivation of this thesis is the lack of comparative analyzes of different thermal management systems in a $LaNi_5$ based metal hydride tank in the literature.
- A hybrid thermal management system is proposed and numerically studied. Rather than a continuous flow inside the cooling channel, a dynamic controller is implemented into the code to activate the heat transfer fluid based on the metal hydride bed temperature.

2.7 Objective

The leading purpose of the thesis is to investigate the storage performance, bed temperature and weight ratio of the PCM integrated $LaNi_5$ based metal hydride tank in the absorption process using MATLAB software. As a result of the obtained storage performance, it is vital for ongoing studies to determine the hydrogen storage amount of the metal hydride tank in various uses such as hydride reactor and fuel cell cooperation. The objectives of the thesis are listed below:

- Developing 2D axisymmetric model in MATLAB software.
- To perform parametric analysis by integrating different thermal management systems into the hydride bed.
- To investigate high storage performance and perform feasibility studies while applying thermal management systems.

2.8 Thesis Outline

In the second chapter, hydrogen storage methods, extensive research on metal hydride, and general sorption processes of metal hydrides are introduced. Information about mathematical model approaches and thermal management systems for the storage of metal hydride is given.

In the third chapter, thermal management systems that determine the storage criteria of metal hydride are introduced and mathematical model approaches are presented. In the discussion part, hydride bed storage performance for each thermal management system is performed by parametric analysis.

In the conclusion part, the pros and cons of thermal management systems are determined, and feasible situations are revealed.

CHAPTER THREE
MATHEMATICAL MODEL

3.1 Methodology

The storage performance of metal hydrides is strongly dependent on thermal management system applicability. In the absorption process, the removal of heat from the hydride bed as a result of the exothermic reaction increases the storage performance. In the thesis, the storage performance of the $LaNi_5$ based metal hydride hydrogen storage tank is compared using different thermal management systems (PCM, external forced convection, cooling channel).

In this part, the mathematical modeling of the hydride bed is introduced for different thermal management scenarios. System description, model reductions, governing equations, boundary conditions, solution method and model validation for external forced convection, phase change material and cooling channel are presented respectively.

3.2 System Description

In this section, $LaNi_5$ based metal hydride hydrogen storage tank is presented with the model structures. Three different thermal management scenarios were examined with external convection (**Scenario -** 1), with PCM (**Scenario -** 2), and with PCM-cooling channel (**Scenario -** 3). The model structures created for each scenario are given in Figure 3.1.

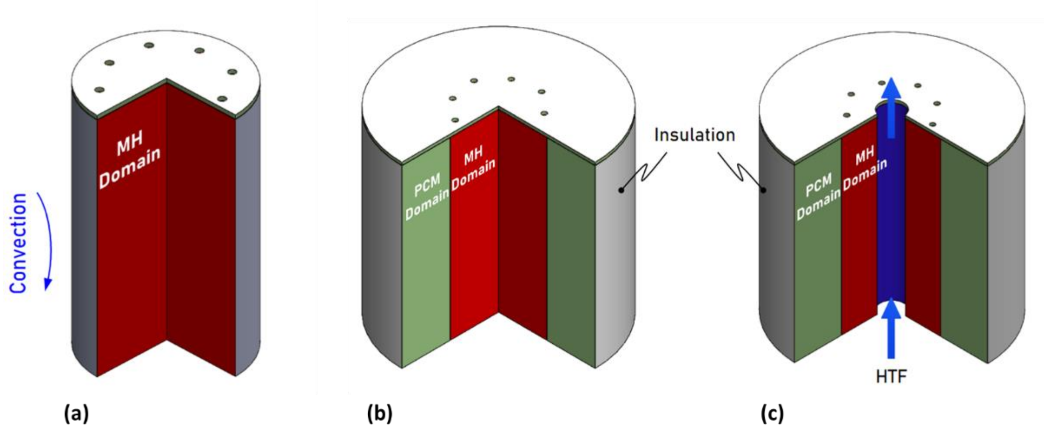

Figure 3.1 3D Model Structure (a) Scenario – 1 (b) Scenario – 2 (c) Scenario – 3

3.2.1 System with external forced convection (Scenario – 1)

A 2D axisymmetric mathematical model was constructed. Convection condition is active on the lateral surface of the tank and is neglected on the bottom surface of the tank (Miled et al., 2017). The entrance of hydrogen into the tank was considered uniform. It is assumed that there is no contraction or expansion at the tank inlet. In Figure 3.2, schematic of the ***Scenario***-1 is given. The radius of the MH tank, R_{MH}, is 2 cm and the height, H_{MH}, is 5 cm.

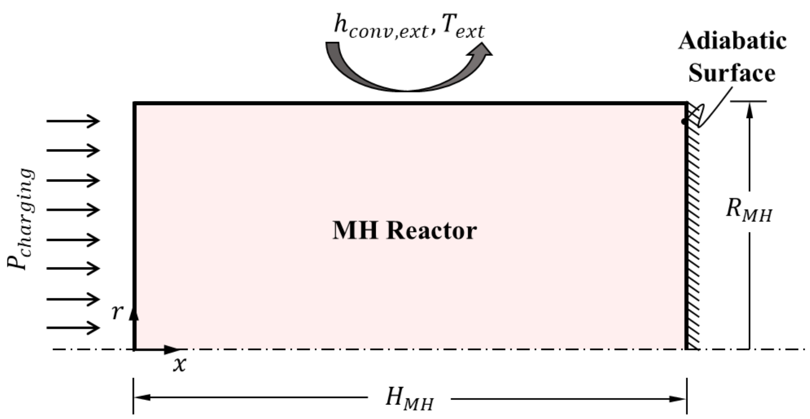

Figure 3.2 Schematic of Metal Hydride Tank (Scenario-1)

3.2.2 *System with PCM and PCM-cooling channel (Scenario-2 and Scenario-3)*

The 2D axisymmetric model of the hydride bed with PCM and cooling channel integrated can be seen in Figure 3.2. Paraffin (T_m = 25 °C), which was observed to be appropriate with $LaNi_5$ metal powder as a result of the literature research, was chosen as the PCM material (Tong, Xiao, Yang, et al., 2019). The cooling channel positioned in the middle of the hydride reactor is an additional thermal management system that includes scenario-2 and scenario-3.

In Scenario 2, the thermal management strategy is provided by PCM only. The cooling channel module in Figure 3.3. is adiabatic.

In Scenario 3, When the mean temperature of metal hydride reactor exceeds 30 °C, the cooling channel is activated, and the heat transfer fluid starts to cool the hydride bed. Eventually, it is aimed to increase the charging performance of the tank. Internal cooling is provided by defining convection to inner wall of the MH tank $(r = R_{tube})$ seen in Figure 3.3. The radius and height of the MH tank are considered the same as scenario-1. The radius of the straight pipe is 0.5 cm and the thickness of the PCM is 2.5 cm.

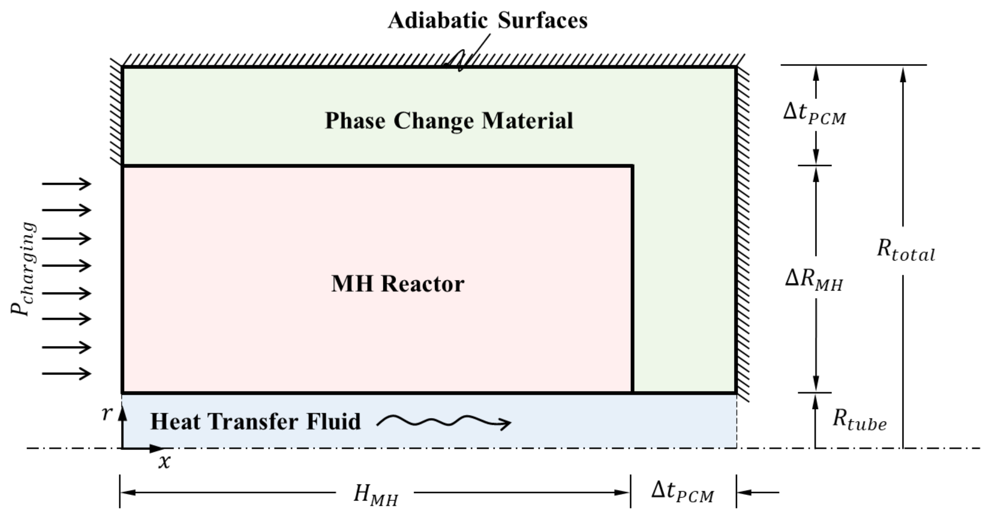

Figure 3.3 Schematic of Metal Hydride Tank (Scenario-2 and Scenario-3)

3.3 Model Reductions and Assumptions

Mathematical models of the MH tank and PCM were introduced in this section. Some simplifications are observed in line with the work of Nasrallah & Jemni (Nasrallah & Jemni, 1997). Thus, a single local temperature was implemented for the entire hydride domain. Pressure changes due to the position have been neglected. The change in the weight fraction in the plateau region in the PCT curve is considered constant (Nasrallah & Jemni, 1997). Since the physics applied to the model allows for symmetry, it was modeled 2D axisymmetric instead of 3D for each scenario. The following assumptions also were considered while modeling the MH tank:

- Thermophysical properties of MH and PCM are constant (Askri, Jemni & Nasrallah, 2003).
- Radiation is neglected for hydride bed (Ye, Lu, Ding, Wang & Yan, 2020).
- The hydrogen is recognized as an ideal gas (Nasrallah & Jemni, 1997).
- Heat conduction is considered in PCM domain (Nasrallah & Jemni, 1997).
- Thermal balance state between the gas and solid phases inside the hydride bed is defined.
- The initial pressure of the MH tank is set to 1.43 bar (Tong, Xiao, Bénard, et al., 2019)
- The initial hydride temperature is assumed to be 25 °C.

3.4 Governing Equations

Conservation of mass, energy balance and chemical reactions are presented in this section for hydride bed, PCM domains respectively. In addition, the equations for enhancing the thermal conductivity of PCM will be presented.

3.4.1 Equations of MH Bed

It is assumed that the ratio of hydrogen, porosity of the hydride bed and metal volumes are constant in each control volume created in the mathematical model. Based on this approach, the mass conservation equation in the tank is given below for the hydrogen and metal regions, respectively.

$$\varepsilon \frac{\partial \rho_g}{\partial t} = -\dot{m}''' \tag{3.1}$$

$$(1-\varepsilon)\frac{\partial \rho_s}{\partial t} = \dot{m}''' \tag{3.2}$$

where, ρ_g density of the hydrogen gas, ρ_s density of the hydride bed, ε is the porosity of the hydride bed and $\dot{m}'''$ is the amount of hydrogen taken up by the hydride per unit time.

The energy equation in cylindrical coordinates system is given as follows,

$$\begin{aligned}(\rho c_p)_{eff} \left(\frac{\partial T}{\partial t}\right) \\ = \frac{1}{r}\frac{\partial}{\partial r}\left(r k_{eff} \frac{\partial T}{\partial r}\right) + \frac{\partial}{\partial x}\left(k_{eff} \frac{\partial T}{\partial x}\right) \\ - \dot{m}'''\left[\Delta H^0 + T\left(c_{p,g} - c_{p,s}\right)\right]\end{aligned} \tag{3.3}$$

where, ΔH^0 is the formation enthalpy, k_{eff} is the effective thermal conductivity and $(\rho c_p)_{eff}$ is the effective heat capacity. k_{eff} and $(\rho c_p)_{eff}$ can be derived from Equation (3.4) and (3.5) as follows,

$$(\rho c_p)_{eff} = \varepsilon \rho_g c_{p,g} + (1-\varepsilon)\rho_s c_{p,s} \tag{3.4}$$

$$k_{eff} = \varepsilon k_g + (1-\varepsilon) k_s \tag{3.5}$$

Hydrogen amount in hydride mass per unit time is determined by the reaction equation,

$$\dot{m}''' = C_a \, exp\left[-\frac{E_a}{R_g T}\right] ln\left(\frac{P_g}{P_{eq}}\right)[\rho_{sat} - \rho_s] \tag{3.6}$$

where, C_a is the time constant, E_a is the activation energy, R_g is the ideal gas constant, T is the temperature of the hydride bed, P_g is the charging pressure, ρ_{sat} is the density of the hydride bed at saturation state, and ρ_s is the metal hydride density. P_{eq} is the equilibrium pressure for absorption process which can be named as derived Van't Hoff Equation (3.7) as follows (Tong, Xiao, Yang, et al., 2019),

$$ln\left(\frac{P_{eq}}{P_{ref}}\right) = A - \frac{B}{T} \tag{3.7}$$

where, A and B are coefficients of Van't Hoff equations and P_{ref} is reference pressure. The variation of the equivalent pressure depending on the absorption temperature is given in Figure 3.4. The equivalent pressure curve increased geometrically at temperatures above the plateau pressure threshold.

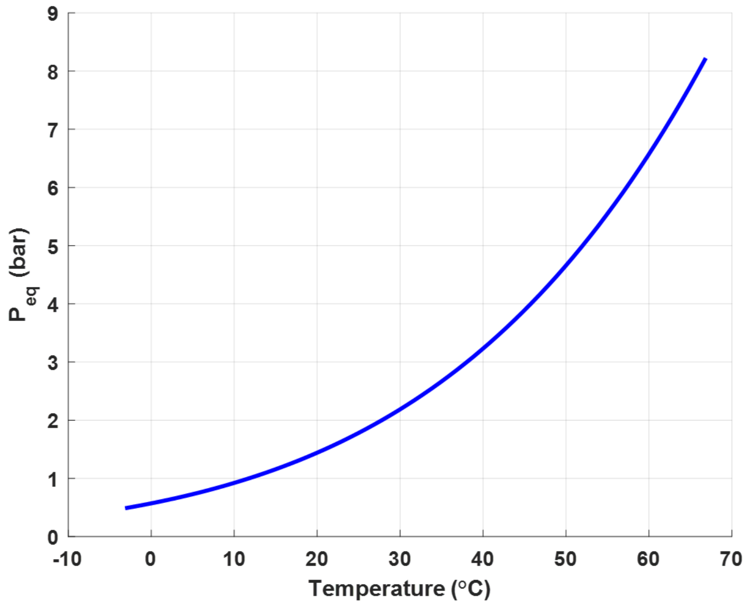

Figure 3.4 Relationship between Equilibrium Pressure and Operating Temperature for AB5 Type Hydride Bed

In the hydride reactor, the charging pressure and the bed temperature affect the volumetric heat generation and the volumetric flow. Variations of these effects at different charge pressures are presented in Figure 3.5. According to the outputs of these analysis, parametric analyzes presented in the next section are performed.

Here, the charge pressure is varied between 2 bar and 10 bar and the analysis is performed for the bed temperature of 290 K and 330 K. It can be traced from the PCT curve that the equivalent pressure increases with the increase of the bed temperature. For this reason, in the analyzes at 330 K, the reaction kinetics at 2, 4 and 6 bar charge pressures do not occur due to the high temperature, because the pressure is not at the desired level. In addition, it can be observed that the hydride bed temperature is at an optimum level for better storage performance, depending on their volumetric heat generation performance. As a result of the temperature parameter in the kinetics reaction equation at 290 K, volumetric heat production is higher than 330 K cases.

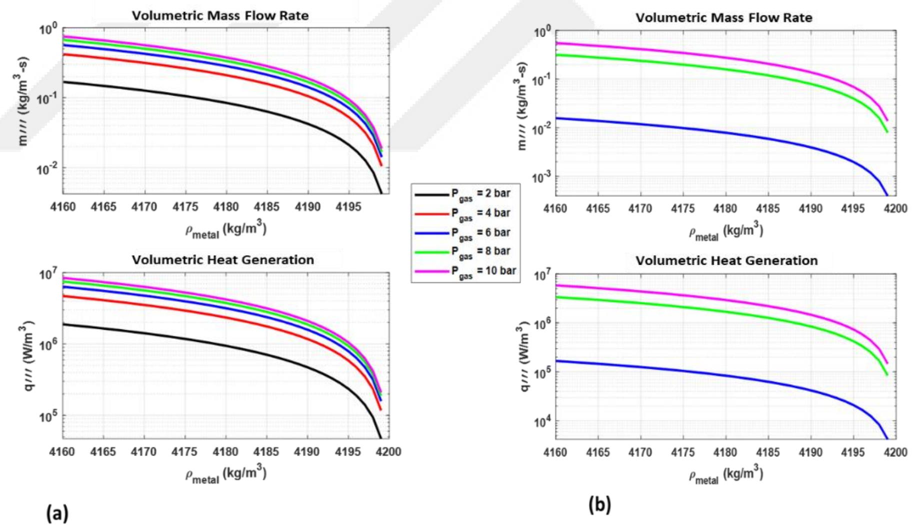

Figure 3.5 Parameters of Volumetric Mass Flowrate and Volumetric Heat Generation depends on Hydride Bed Temperature (a) 290 K (b) 330 K

3.4.2 Equations of PCM

In the PCM model, heat conduction is defined by the temperature conversion method. According to this method, the solidification process takes place in the mushy phase in the range of $2\delta T_m$. In Figure 3.6, the enthalpy-temperature relationship is introduced for the solid, mushy and liquid phases. The PCM energy balance in equation 3.8 is as follows,

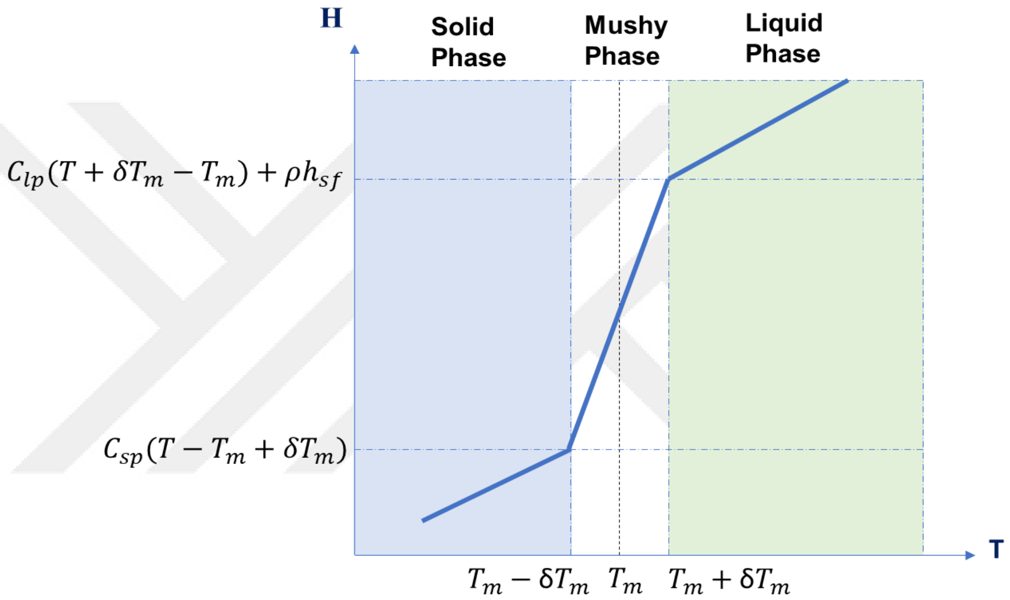

Figure 3.6 Relationship Between Enthalpy and Temperature

$$\frac{\partial C}{\partial t} = \frac{1}{r}\frac{\partial}{\partial r}\left(k_{en} r \frac{\partial T}{\partial r}\right) + \frac{\partial}{\partial x}\left[k_{en}\frac{\partial T}{\partial x}\right] - \frac{\partial S}{\partial t} \tag{3.8}$$

where k_{en} is the enhanced thermal conductivity, S is the source term of the reaction. The coefficients C and S can be expressed for solid,mushy and liquid phases in Equation (3.9) and (3.10) as follows (Dincer & Ezan, 2018),

$$C(T) = \begin{cases} C_{sp} & T < T_m - \delta T_m \\ C_{mp} + \rho \dfrac{h_{sf}}{2\delta T_m} & T_m - \delta T_m \leq T \leq T_m + \delta T_m \\ C_{lp} & T > T_m + \delta T_m \end{cases} \tag{3.9}$$

$$S(T) = \begin{cases} C_{sp}(\delta T_m - T_m) & T < T_m - \delta T_m \\ \left(C_{mp} + \rho \dfrac{h_{sf}}{2\delta T_m}\right)(\delta T_m - T_m) & T_m - \delta T_m \leq T \leq T_m + \delta T_m \\ C_{lp}\delta T_m - C_{lp}T_m + \rho h_{sf} & T > T_m + \delta T_m \end{cases} \tag{3.10}$$

where, T_m is the melting temperature, δT_m is the melting temperature range. General solver steps which include equilibrium pressure, volumetric mass flow rate equation, mass conservation, energy balance and Faghri equations are defined in Figure 3.7.

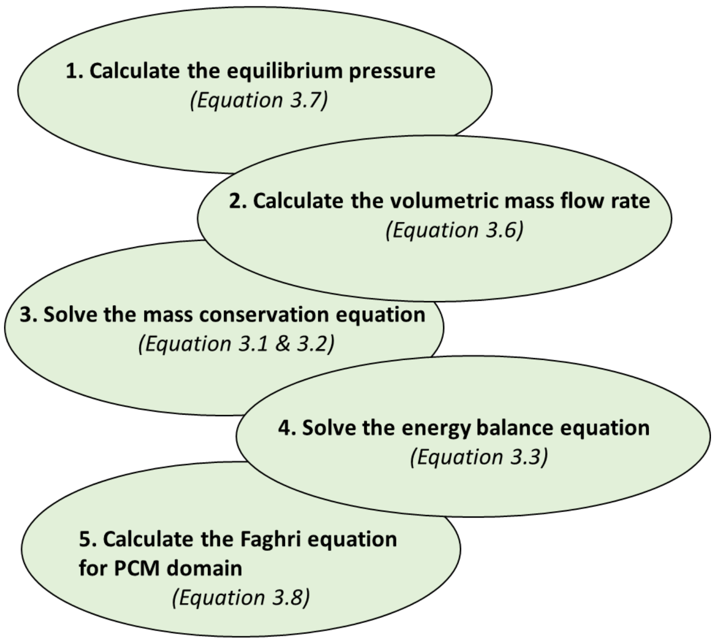

Figure 3.7 General Solver Steps

The thermal conductivity coefficient of PCM where, chosen in the litarute, is between 0.24-2 (W/m-K). As a result, enhancing the thermal conductivity accelerates the melting and solidification processes. The correlations of natural convection in the cylindrical cavity of the MH tank were used to increase liquid PCM conductivity. For this, the ratio of the increased thermal conductivity to the constant PCM conductivity was obtained in Equation 3.11 by using Nusselt correlations (Cengel & Ghajar, 2015),

$$Nu = \frac{\mathrm{k}_{en}}{k_{PCM,l}} = 0.386\left(\frac{Pr}{0.861 + Pr}\right)\left(F_{cyl}Ra_L\right)^{\frac{1}{4}} \tag{3.11}$$

where, Pr is Prandlt number, Ra is the Rayleigh number. These dimensionless parameters can be calculated as follows,

$$Pr = \frac{\mu c_p}{k} \tag{3.12}$$

$$Ra_L = \frac{g\beta(T_{ave} - T_{melting})L_c^3}{\vartheta\alpha} \tag{3.13}$$

where, g is the gravitational acceleration, β is the expansion coefficient, ϑ is the kinematic viscosity, α is the thermal diffusivity, μ is the dynamic viscosity. In addition, geometry coefficient F_{cyc} can be described as follows (Cengel & Ghajar, 2015),

$$F_{cyc} = \frac{\ln\left(\frac{D_o}{D_i}\right)^4}{L_c^3\left(D_i^{-\frac{3}{5}} + D_o^{-\frac{3}{5}}\right)^5} \tag{3.14}$$

where, D_o and D_i are the interior and exterior diameter of the cylindrical geometry, L_c is the characteristic distance between two cylinders.

3.5 Boundary Conditions

Boundary conditions in the designed mathematical model are shown in Table 3.1 for 3 different scenarios. When the cooling channel is active (scenario 3), The heat transfer fluid is located on the bottom surface of the tank and cools the tank with a certain temperature and convection coefficient. When only PCM configuration (scenario 2), the cooling channel is designated as the adiabatic wall. The generalized model for the 3 scenarios is presented in Figure 3.8.

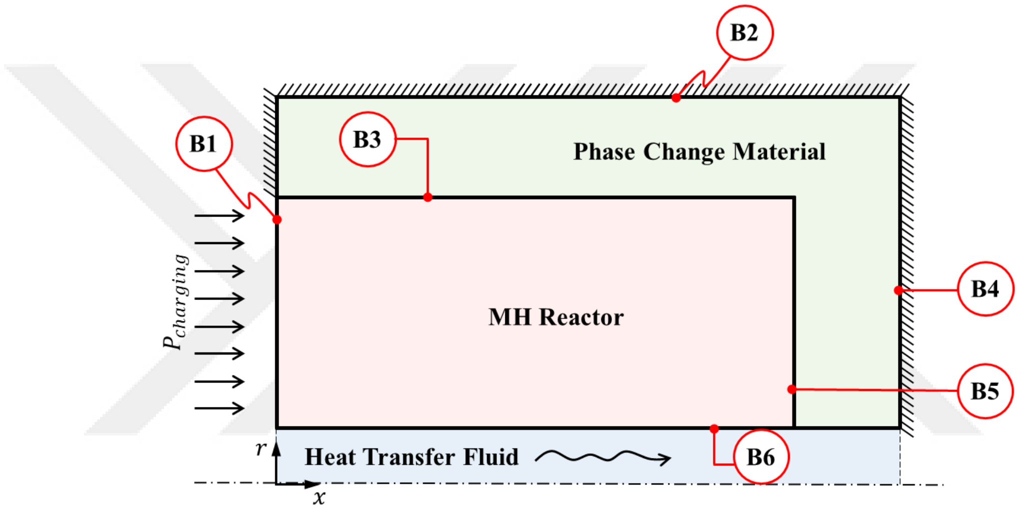

Figure 3.8 Boundary Conditions for Each Scenario

Table 3.1 Boundary Conditions According to Surfaces

Scenario	B1 (Top)	B2 (Lateral)	B3 (Lateral)	B4 (Bottom)	B5 (Bottom)	B6 (Inner surface of the pipe)
1	Pressure inlet	N/A	External Convection	N/A	Adiabatic	N/A
2	Pressure inlet	Adiabatic	PCM interface	Adiabatic	PCM/MH Reactor interface	Adiabatic
3	Pressure inlet	Adiabatic	PCM interface	Adiabatic	PCM interface	Heat transfer fluid

3.6 Solution Method

A 2D axisymmetric model was constructed in MATLAB software. In the analyzes created with the finite volume method and explicit scheme in the 0.001 second time step and 1000 meshes for the MH domain and 3500 meshes for the PCM domain were used in Scenario 2 and Scenario 3. In Scenario 1, 1600 meshes were used. Depending on the hydride bed temperature, for critical situations, cooling channel domain is defined as the heat transfer fluid or adiabatic boundary conditions. Growth rate was not used during validation because the error rate of the uniform mesh was below 0.5%. Mesh images in MATLAB environment for scenario 1 and scenario 2-3 were defined in Figure 3.9 and Figure 3.10 respectively.

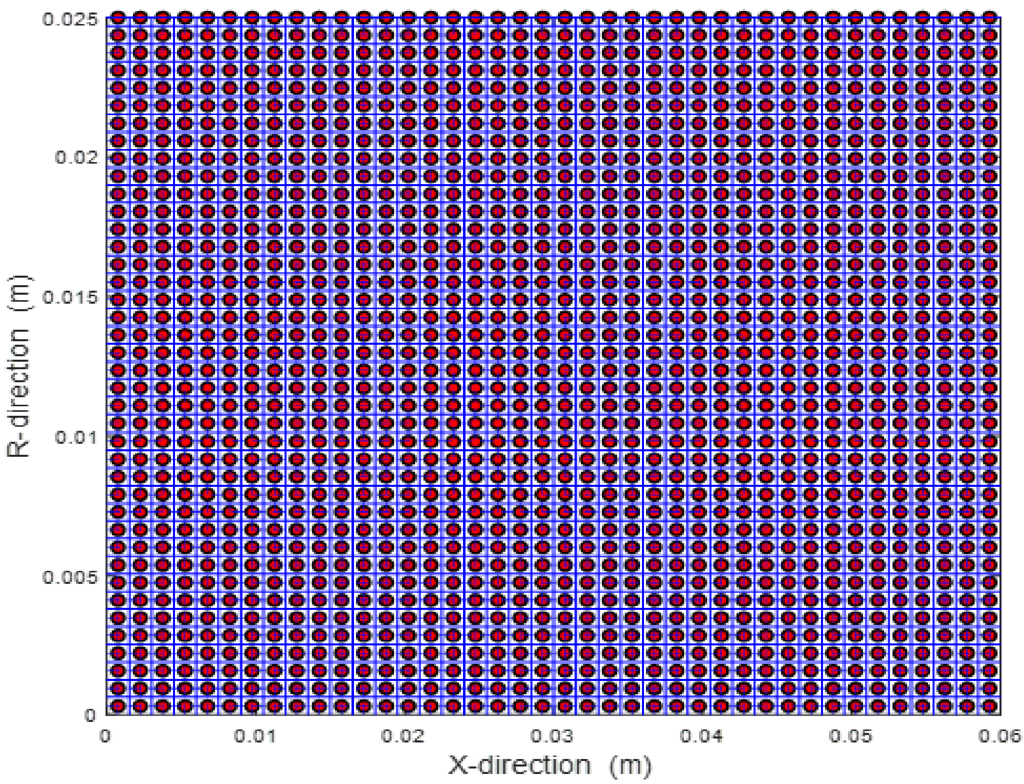

Figure 3.9 Mesh Image for Scenario 1 (Hydride Domain)

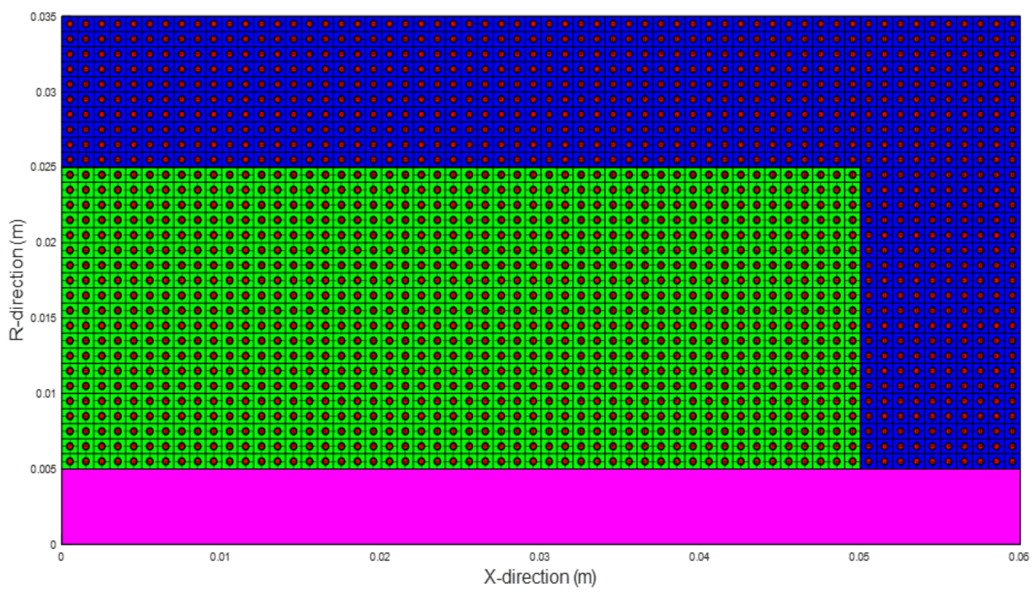

Figure 3.10 Mesh Image for Scenario -2 and Scenario -3 (Blue: PCM Domain, Green: Hydride Domain, Pink: HTF Domain)

3.7 Model Verification

The consistency of the current model is tested by regenerating the numerical model of Tong et al. (Tong, Xiao, Yang, et al., 2019). They developed a CFD model in COMSOL for the thermal management of absorption processes for external and dual (internal and external) cooling modes. The model does not include a cooling channel in external cooling mode as in Scenario-1 of the current study. In the dual cooling mode, there is a straight pipe inside the MH reactor, and the excess heat generated during the absorption reaction is extracted through the external and internal fluids. Two modes that are used in Tong's paper are reproduced in MATLAB by disregarding the velocity field and spatial variations of pressure inside the tank. Figure 3.10 compares the variations in weight fractions and average MH tank temperatures that are obtained in the reference study and the current model. Here the external cooling mode is labeled *as w/o pipe*, and the dual cooling mode, which allows heat transfer through the outer wall and the fluid passing through the tube, is marked as *w/pipe*. It is clear that the current model successfully captures the numerical outputs of the reference paper both with and without pipe configurations.

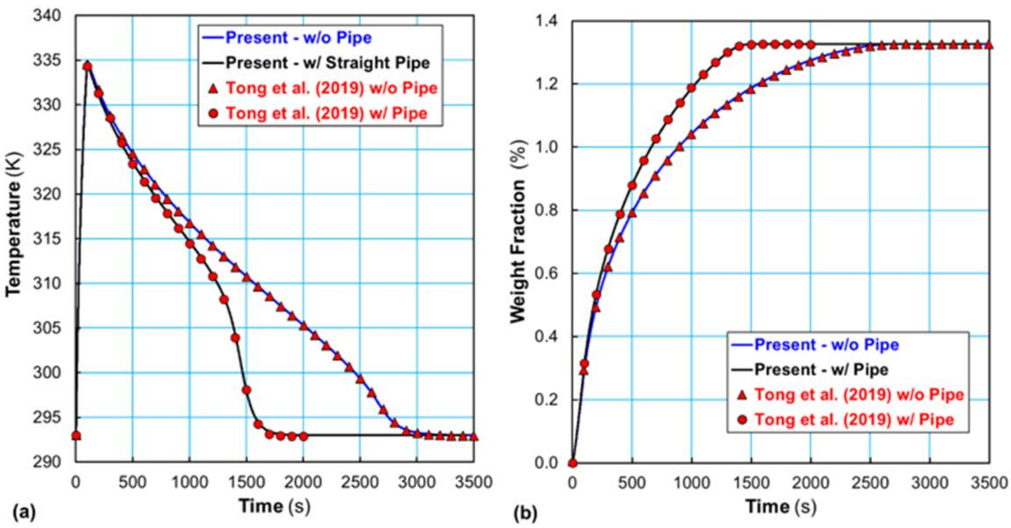

Figure 3.11 Model Verification with Tong et al. (Tong, Xiao, Yang, et al., 2019)

CHAPTER FOUR
RESULTS AND DISCUSSION

4.1 Investigations on Parametric Analyzes and Parameter Types

After the model is verified, parametric analyzes will be made and the effects of storage of the $LaNi_5$ based hydride tank, hydride tank temperature, temperature changes depending on the position, and the storage percentage and duration of different thermal management systems will be examined.

This chapter covers the examination of various thermal management systems with their specific parameters. Based on the scenarios (i) external forced convection thermal management system (ii) thermal management system of PCM (Paraffin usage) entegration with MH tank (iii) system with cooling channel and PCM introduced in the previous chapter, analyzes will be presented. In addition, a comparative review of each thermal management scenario will be observed.

Thermophysical properties, reaction, and chemical equation coefficients of hydride bed and PCM are given in Table 4.1. It is clear that the hydride material has a certain temperature limit. The melting temperature of the Paraffin material used in PCM selection is determined according to the maximum temperature level of the hydride tank. In this section, different analyzes were performed for PCM melting temperature and it was observed that the maximum tank temperatures remained at the desired level at 25°C melting temperature and optimum thermal management was achieved.

When examining more than one parameter for three different thermal management scenarios, it is necessary to set the constant parameters appropriately. Therefore, only the effects of the changed parameters are intended to be observed. The parameters taken as constant in the parametric analysis are given in Table 4.2.

Table 4.1 Thermophysical Parameters of MH Tank and PCM (Tong, Xiao, Yang, et al., 2019).

	Parameters	Value
Metal Hydride Tank	Metal density, ρ_s [kg/m³]	7164
	Saturated density of MH, ρ_{ss} [kg/m³]	7259
	Heat Capacity of MH tank, $c_{p,MH}$ [J/kg-K]	419
	Thermal Conductivity of MH tank, k_{MH} [W/m-K]	2.4
	Activation Energy for Absorption, E_a [J/mol]	21179.6
	Reaction Constant, C_a [1/s]	59.187
	Porosity, ε [-]	0.5
	Maximum Weight Fraction, $\%wt$	1.32
	Enthalpy of Reaction, ΔH [J/kg]	1.537×10^7
	Absorption Plateau Pressure Coefficient, A [-]	10.57
	Absorption Plateau Pressure Coefficient, B [K]	3074.6
	(*) Charging Pressure, [bar]	8
Phase Change Material (Paraffin)	PCM Density, ρ_{PCM} [kg/m³]	880
	Heat Capacity of PCM, $c_{p,PCM}$ [J/kg-K]	2100
	Thermal Conductivity of PCM, k_{PCM} [W/m-K]	0.2
	(*) Latent Heat of Fusion, ΔH_{PCM} [kJ/kg]	150
	Melting temperature, T_m [K]	298
	Dynamic Viscosity, μ [kg/m-s]	3.86×10^{-3}

(*) When not used in parametric analysis, the value of the parameter in the table is taken as a constant.

Table 4.2 Constant Parameters for Each Scenario

Parameters	**Scenario**	**Value**
Charging pressure, P_{inlet} [bar]	1-2-3	20
External temperature, $T_{external}$ [°C]	1	25
PCM thickness, t_{PCM} [m]	2-3	0.025
Latent heat of PCM, ΔH_{PCM} [J/kg]	2-3	150000
Convective heat transfer coefficient inside the pipe, $h_{conv,pipe}$ [W/m²K]	3	5000
External Convective heat transfer coefficient, $h_{conv,scenario-1}$ [W/m²K]	1	500
Temperature of heat transfer fluid, T_{fluid} [°C]	3	0
PCM melting temperature, $T_{melting}$ [°C]	2-3	25
Temperature limit (for opening the cooling channel domain), T_{lim} [°C]	3	30
Porosity, ε [-]	1-2-3	0.5

As a result of parametric analysis, in general, full storage time, weight ratio for specific time periods, positional temperature distributions are discussed. It is aimed to determine feasible parameters and scenarios for fast and complete storage. 379 different analysis results were shared in Table 4.3.

Table 4.3 Selected Parameters for Three Different Scenarios

Variables	Major Outputs	Number of Analyzes		
		Scenario 1	**Scenario 2**	**Scenario 3**
Convective heat transfer (external condition)	Bed temperature - weight fraction	18	N/A	N/A
External temperature and convective heat transfer	Charging at t=300 s (%)	100	N/A	N/A
PCM thickness	Bed temperature - weight fraction	N/A	18	18
Latent heat	Bed temperature - weight fraction	N/A	18	18
PCM thickness and latent heat	Bed temperature - weight fraction	N/A	72	N/A
Heat transfer fluid – convective heat transfer (cooling channel)	Charging at t=300 s (%)	N/A	N/A	72
Porosity	Charging time	5	N/A	N/A
Charging pressure – hydride bed tempreature	Charging time	24	16	N/A
				Total Analyzes: 379

4.2 Active Thermal Management with External Forced Convection (Scenario 1)

In this thermal management scenario, the effect of parameters such as external temperature, porosity, charge pressure, external convection coefficient on the storage criteria will be examined. The model belonging to the scenario (Figure 3.1) was introduced in the previous chapter.

4.2.1 Influence of Convective Heat Transfer Coefficient under Different Charging Pressure

The effect of the external convective heat transfer coefficient on the time-wise variations in the weight fractions and the tank temperatures are represented in Figure 4.1 at charging pressures of 10 bar, 20 bar, and 30 bar. With the increasing convective heat transfer coefficient, the storage time reduces. Complete charging is obtained in all *cases* except for the *case* with a charging pressure of 10 bar and a convective heat transfer coefficient of 100 W/m^{2}K. At a charging pressure of 30 bar, the complete charging time reduces from 2612 seconds to 1218 seconds when the convective heat transfer coefficient is increased from 100 W/m^{2}K to 5000 W/m^{2}K. As depicted in

Figure 4.1(b), the mean temperature of the MH tank is also affected by the convective heat transfer, and the peak temperature significantly reduces when the convective heat transfer coefficient is enhanced. When the convective heat transfer coefficient is defined as 100 W/m^2K the peak MH tank temperatures are obtained to be 72°C, 95°C, and 112°C for charging pressures of 10 bar, 20 bar, and 30 bar, respectively. At 20 bars, the maximum hydride bed temperature reduces from 97°C to 85°C when the heat transfer coefficient is improved from 100 W/m^2K to 5000 W/m^2K, by 50 times. It is observed in Figure 4.1(a) inset image that increasing the charging pressure accelerates the charging process, and the weight fraction significantly improves in the early periods. For a selected convective heat transfer coefficient, e.g., 5000 W/m^2K, at the end of 100 s, weight fractions are obtained as 0.35%, 0.5%, and 0.58% for 10, 20, and 30 bars, respectively. Besides, considering the effect of the convection heat transfer coefficient at the early periods of the process, e.g., at 100 s, the increment from 100 W/m^2K ($wt\%$ = 0.22) to 5000 W/m^2K ($wt\%$ = 0.58) at 30 bars, the weight fraction increases by 263%.

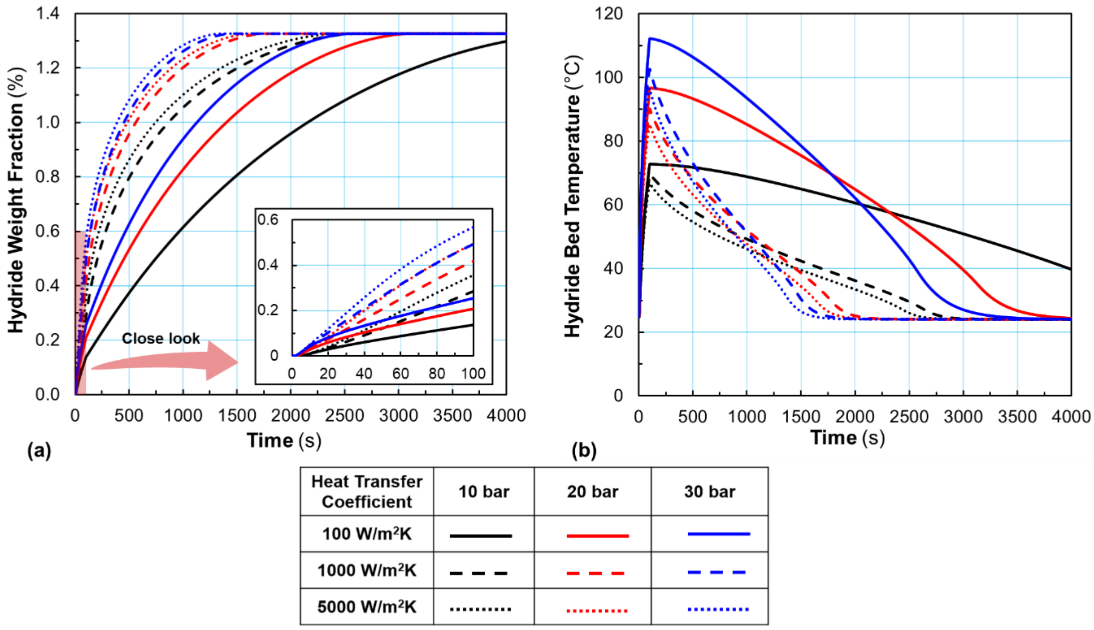

Figure 4.1 Effect of Convective Heat Transfer Coefficient on the Time-Wise Variations of (a) Weight Fraction (b) MH Tank Temperature

4.2.2 Influences of External Temperature and Convective Heat Transfer Under Different Charging Pressures

The percentage of the stored hydrogen inside the container is used to concisely compare the results obtained from a large set of simulations. The storage percentage is defined as the fraction of the *wt%* at t = 300 s to the maximum allowable *wt%* of the MH reactor. The influences of parameters on the storage percentage are provided in Figure 6 for two charging pressures of 10 and 30 bar. Figure 4.2 includes 100 parametric results representing external temperature, convection coefficient, and charging pressure interaction. Figure 4.2(a) and (b) reveal that the storage percentage hardly depends on the charging pressure and convective heat transfer coefficient. Maximum storage is provided when the external convective heat transfer coefficient is the highest and the external temperature is the lowest. Maximum storage percentages are obtained at 59.6% and 74.5%, at 10 bar and 30 bar, respectively. It should be noted that the external temperature has a minor effect on the stored hydrogen in the current range of parameters. One should also notice that variations in convective heat transfer are effective for relatively low convection values, i.e., less than 1000 W/m^{2}K. At lower heat transfer coefficients, the convective resistance on the tank's outer surface significantly influences the reaction. However, further enhancing the convective heat transfer coefficient makes the thermal resistance associated with the convection negligible, and the results become almost independent from the convective heat transfer coefficient variations.

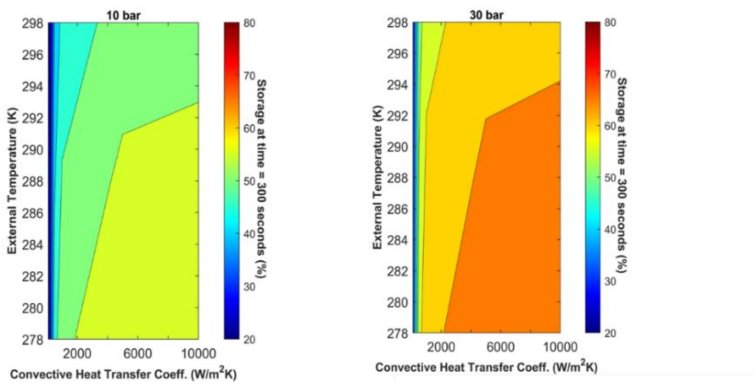

Figure 4.2 Effects of External Temperature and Convective Heat Transfer Coefficient on the Storage Percentage at the end of 300 s with Charging Pressures (a) P = 10 bar (b) P = 30 bar

4.2.3 Influence of Charging Pressure, Hydride Bed Temperature and Porosity on Full Storage Time

The effect of charge pressure and porosity on the full storage time is presented in Figure 4.3. The maximum hydride temperature for each case can be seen in Figure 4.3(a) and (b).

In Figure 4.3(a), with the enhancement of the charge pressure from 6 bar to 12 bar, the storage time is reduced by 21 minutes. In addition, the hydride temperature increases by 19 K. The charging pressure accelerates the reaction kinetics (Equation 3.6), and the hydride bed temperature rises.

In Figure 4.3(b), the result parameter of porosity on the full storage time is observed. No significant change is observed in storage time and hydride bed temperature with increasing porosity. While the porosity was 0.8, the storage time was reduced approximately by 1 minute compared to lowest porosity case ($\varepsilon = 0.2$). For each comparison, hydride bed temperature was reduced by 2 K. Both reductions can be verifiable by the fact that porosity reduces the hydride volume and reduces the area of reaction effect.

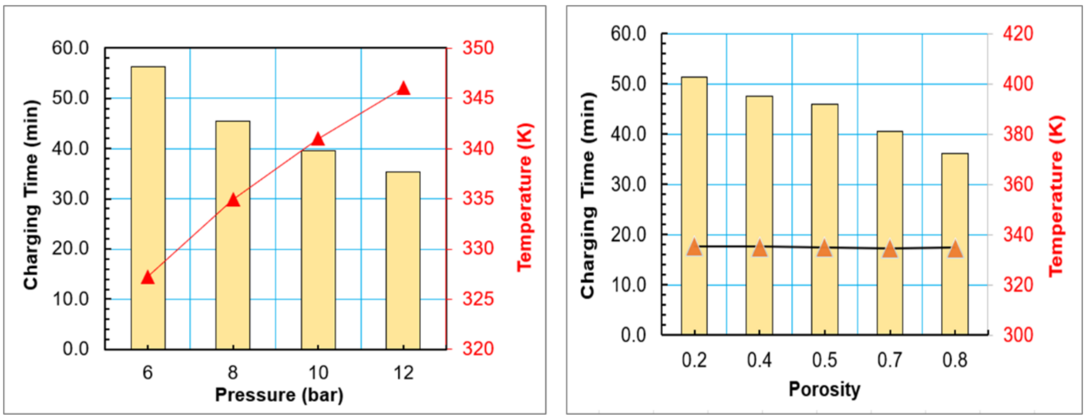

(a) (b)

Figure 4.3 The Effect of Charging Pressure, Porosity and Hydride Bed Temperature on Full Storage Time (a) Charging Pressure – Bed Temperature (b) Porosity – Bed Temperature

4.3 Passive Thermal Management with PCM (Scenario 2)

In this scenario, the effects of PCM will be examined. The walls of the PCM are adiabatic, meaning there is no forced convection. PCM thickness, latent heat, charging pressure, and melting temperature parameters affect overall storage criteria. Accordingly, storage time, hydride temperature and positional distributions will be presented for scenario 2.

4.3.1 Influence of PCM Thickness Under Different Charging Pressure

With a view to investigate the impact of PCM mass on the thermal management performance of an MH absorption process, three different thicknesses of PCM (1 cm, 2.5 cm, and 5 cm) are considered. The charging pressure is changed from 10 bar to 30 bar. The time-wise evolutions in the *wt%* and MH tank temperatures are given in Figure 4.4. It is clear that the amount of PCM is critical to ensure the continuity of the charging process. 1 cm PCM thickness is not sufficient to extract the generated heat from the hydride domain in all charging pressures tested in this study. In less than 500 seconds, the MH tank temperatures reach peak values and remain constant for the rest of the process. Increasing the charging pressure improves the hydrogen's charging fraction and increases the MH tank temperature.

Increasing the PCM thickness to 2.5 cm allows complete storage for supply pressures of 20 bar and 30 bar. However, the limited heat storage capacity of the PCM domain could keep the MH tank temperature as much as 70°C – 80°C. Increasing the PCM thickness to 5 cm accelerates the charging process, and the complete charging is obtained achieved less than 2500 s in all pressures. The higher heat storage capacity of the PCM domain allows it to absorb the heat in the MH domain. The mean MH temperature gradually reduces to the initial temperatures as the charging process finalizes.

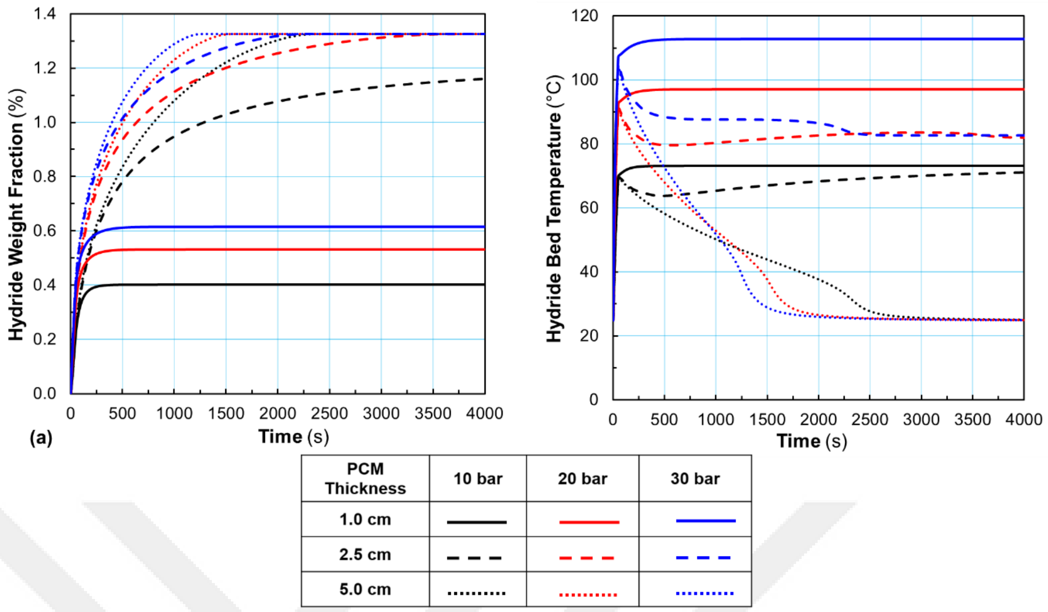

Figure 4.4 Time Dependent (a) Weight Fraction (b) Temperature Graphs at Different Charging Pressures - $T_m = 25$ °C, h_{sf} =150 kJ/kg

4.3.2 Influence of PCM Latent Heat of Fusion under Different Charging Pressure

Figure 4.5 represents the effects of latent heat of fusion of PCM on *wt*% of hydrogen and MH tank temperature at different charging pressures. Results show that increasing the charging pressure or latent heat of fusion of the PCM accelerates the absorption process. Charging with P = 30 bar and h_{sf} = 250 kJ/kg is the fastest method in which the charging process is completed in 1508 s. It should be noted that the effect of latent heat of fusion of PCM becomes more apparent at high charging pressures. At higher charging pressures, i.e., 20 bar and 30 bar, the MH tank temperature increases as much as 90°C - 100°C. Since PCM with a lower latent fusion value has a lower heat storage capacity, the steady-state temperatures depend on the PCM properties. At 10 bar of charging pressure, the hydride bed temperature dropped by 12°C when the latent heat of fusion increased from 100 kJ/kg to 250 kJ/kg. In addition, at higher charging pressures, i.e., 30 bar, the influence of latent heat of fusion on the time-wise evolution of the MH tank temperature becomes more apparent. The reduction in MH tank temperature by increasing the latent heat parameter from 100 kJ/kg to 250 kJ/kg is as much as 32°C at 30 bar charging.

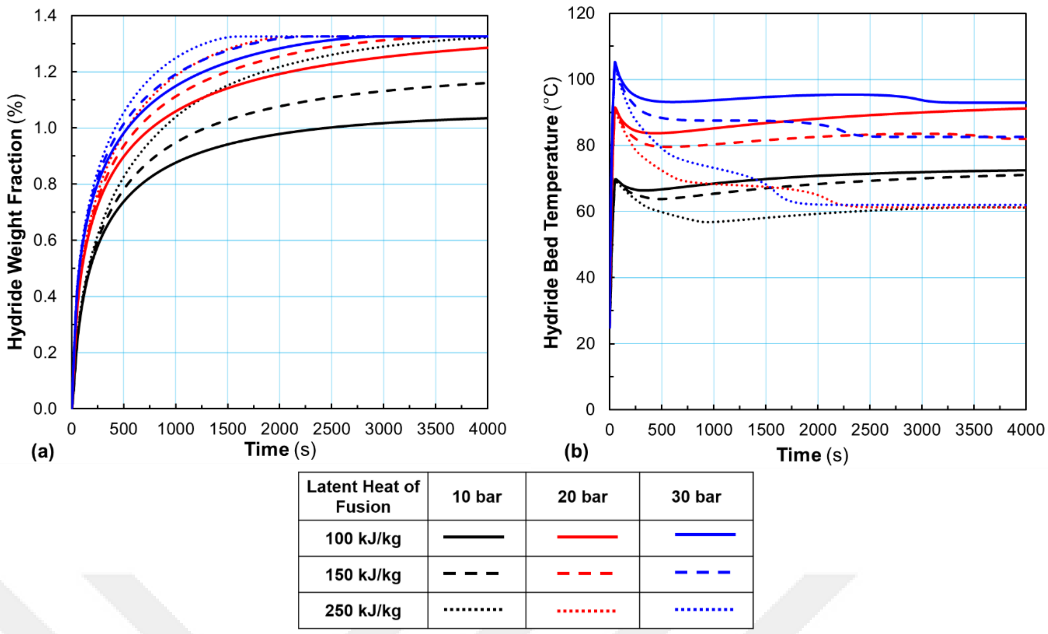

Figure 4.5 Variations in (a) Weight Fraction (b) MH Tank Temperature as a Function of PCM's Latent Heat of Fusion at Different Pressures - (T_m = 25°C, t_{pcm} = 2.5 cm)

4.3.3 The Effect of Latent Heat and PCM Thickness on Charging Percentage under Different Charging Pressure

A total of 40 analyses were conducted to assess the combined effects of PCM's latent heat and thickness on the stored hydrogen at different charging pressures. Figure 4.6 summarizes the results for P = 10 bar and 30 bar at 300 s. It is observed that increasing the PCM thickness and latent heat enhances the stored amount of hydrogen. At P = 10 bar, maximum storage is obtained as 52% at 250 kJ/kg latent heat and 5 cm PCM thickness. Increasing the charging pressure to 30 bar accelerates the charging rate, and higher storage percentages are observed. At 30 bar of charging pressure, the maximum storage percentage is obtained as 74.8%. Variations in PCM thickness do not cause a considerable change in the storage performance significantly beyond 3 cm. The changes in PCM thickness become important at lower latent heat values and PCM thicknesses less than 2.5 cm.

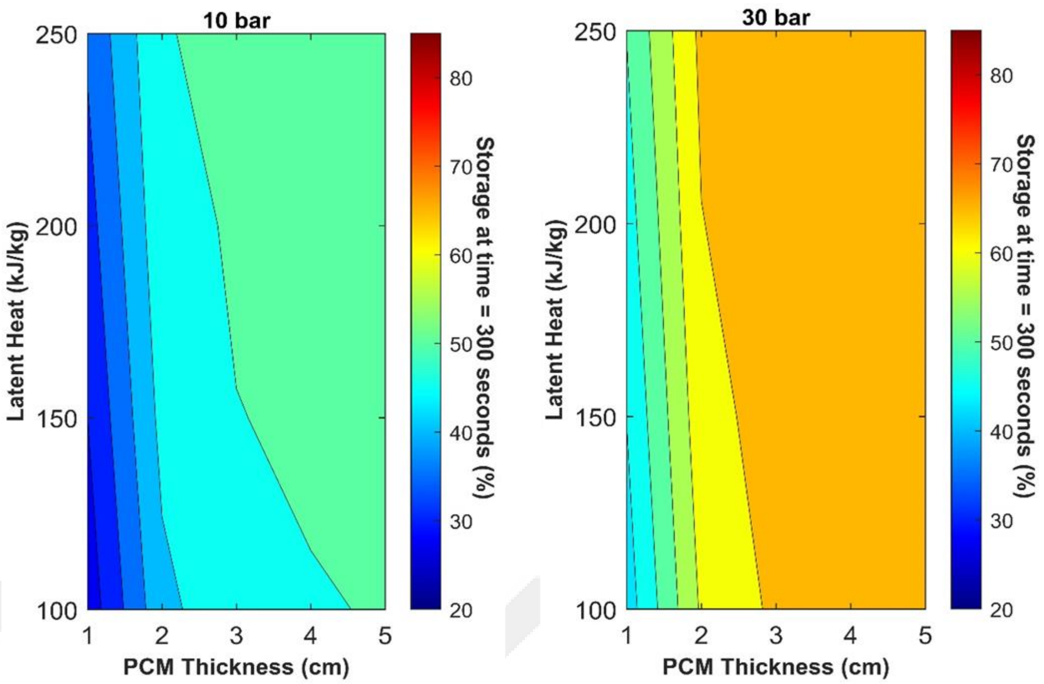

Figure 4.6 Effect of Latent Heat and PCM Thickness on Charging (a) P = 10 (bar) (b) P = 30 (bar)

4.3.4 The Effect of Latent Heat on Positional Hydride Bed Temperature

The effect of PCM latent heat on positional hydride temperature is presented in Figure 4.7 for two-time (time at 300 and 600 s) periods. For time at 600 seconds and 100 kJ/kg latent heat in Figure 4.7(a) and (b), required thermal management for the hydride tank could not be achieved during the absorption process. In addition, as the reaction progresses, hydride bed temperature increases.

The PCM temperature with the hydride temperature during the reaction is 68 °C. At latent heat 250 kJ/kg, the maximum hydride temperature is 61 °C in Figure 4.7(c). As the reaction progresses, a temperature drop is observed for the hydride domain boundary. In contrast, the PCM temperature is 42 °C at the hydride domain boundary. It decreases to 28 °C as it moves away from the hydride domain. For time at 600 seconds, the thermal management performance provided by 250 kJ/kg of latent heat is higher in Figure 4.7(d).

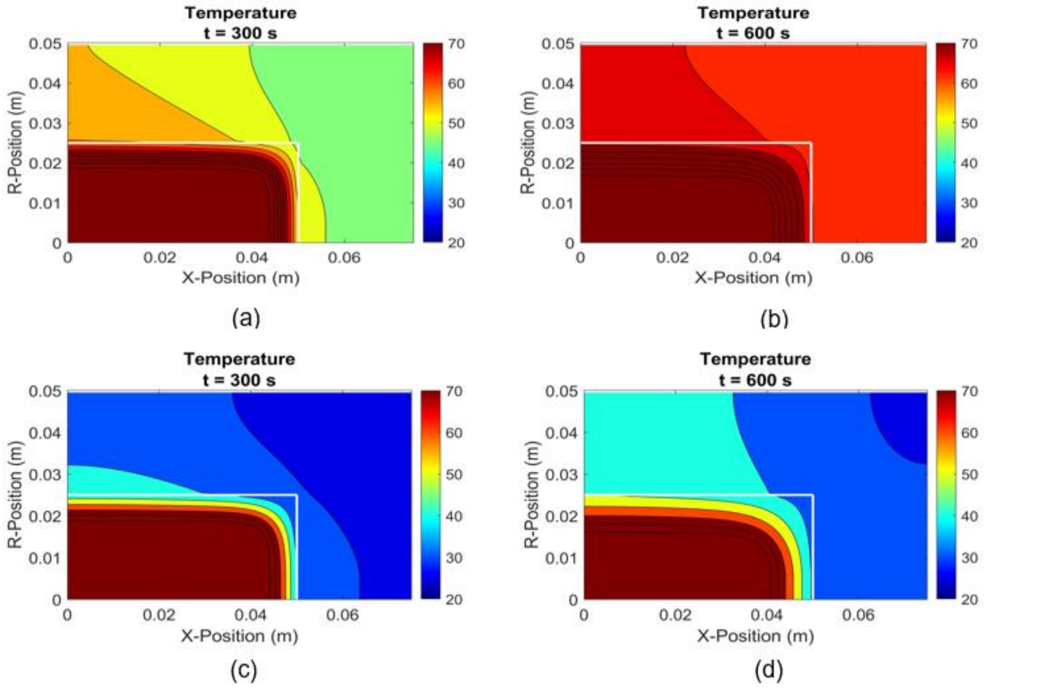

Figure 4.7 Effect of Latent Heat on Hydride Temperature (a) Latent Heat 100 kJ/kg (t = 300 s) (b) Latent Heat 100 kJ/kg (t = 600 s) (c) Latent Heat 250 kJ/kg t = 300 s (d) Latent Heat 250 kJ/kg (t = 600 s)

4.4 Hybrid Thermal Management System Combined with PCM and Cooling Channel (Scenario-3)

In scenario 3, the system with cooling channel tries to reduce the hydride bed temperature by applying a hybrid thermal management strategy together with the PCM. When the hydride bed temperature rises above 30 °C, a heat transfer fluid forces the system to cool through the cooling channel.

In this section, the same analyzes performed for scenario 2 are performed for scenario 3. In addition, scenario comparisons were made in terms of positional temperature distributions and storage criteria.

4.4.1 Influence of PCM Thickness Under Different Charging Pressure (Scenario-3)

The effectiveness of PCM thickness on hybrid bed temperature and weight ratio in the hybrid thermal management system is presented in Figure 4.8. The complete charging is achieved in 480 seconds with a charging pressure of 30 bar and a thickness of 5 cm PCM. At 10 bar of charging pressure and 1 cm of PCM, the time for complete charging increases to 1785 seconds. The inset image in Figure 4.8(b) shows that in the *case* of 10 bar charging pressure and 5 cm PCM thickness, the tank fills faster than the case with 20 bars charging pressure and 1 cm PCM thickness. The amount of PCM is vital for the performance of the hydride reactor in the absorption process. Figure 4.8(b) shows three temperature peaks for three charging pressures. The maximum hydride temperatures are almost identical for the same charging pressures, regardless of PCM thicknesses. The highest hydride bed temperature increases by 36°C when the charging pressure is enhanced from 10 bar to 30 bar. When the PCM thickness is increased by 4 cm at 30 bar charging pressure, the time to attain the bed temperature of 25°C is reduced by 890 seconds.

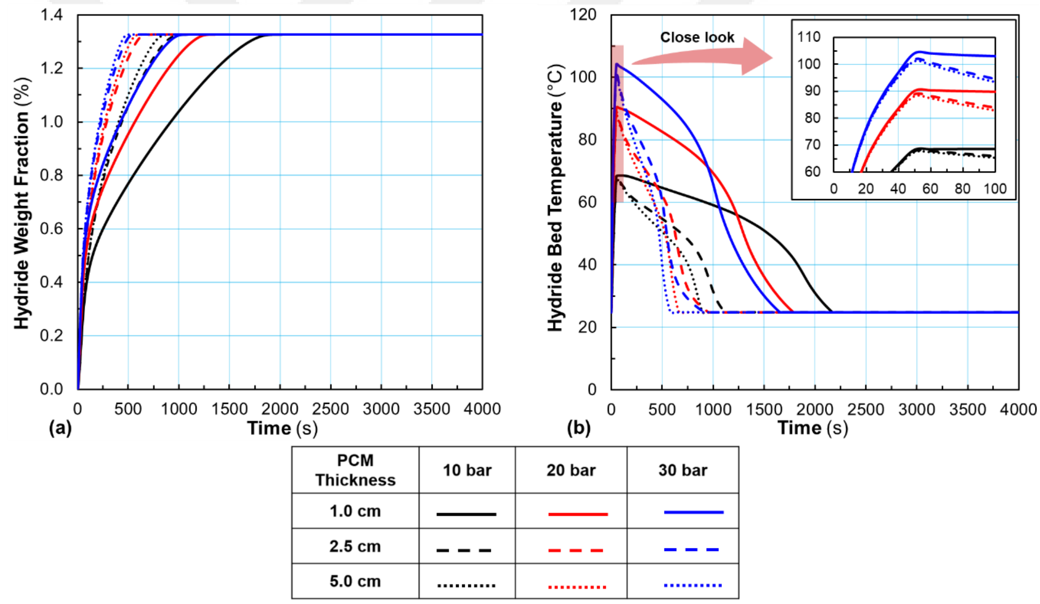

Figure 4.8 Effect of PCM Thickness Under Different Charging Pressure (a) Weight Fraction (b) Hydride Bed Temperature

4.4.2 Influence of Latent Heat of PCM Under Different Charging Pressure (Scenario-3)

The effect of latent heat on weight ratio and hydride temperature evolutions are presented in Figure 4.9 for three charging pressures. According to Figure 4.9(a), it is observed that the maximum filling time is reduced when the latent heat and pressure increase. At P = 10 bar, the time for complete charging is obtained as 1082 seconds for P = 10 bar and h_{sf} = 100 kJ/kg. Increasing the pressure to 30 bar and latent heat to 250 kJ/kg reduces the charging time to 508 seconds. One should note that latent heat value has little impact on the charging time than the charging pressure. The inset image in Figure 4.10(b) implies that the maximum hydride bed temperature does not significantly vary with latent heat value. For each charging pressure, the maximum temperatures are almost identical regardless of the latent heat value, e.g., P = 10 bar – T_{max} = 68°C, P = 20 bar – T_{max} = 88°C, P = 30 bar – T_{max} = 102°C.

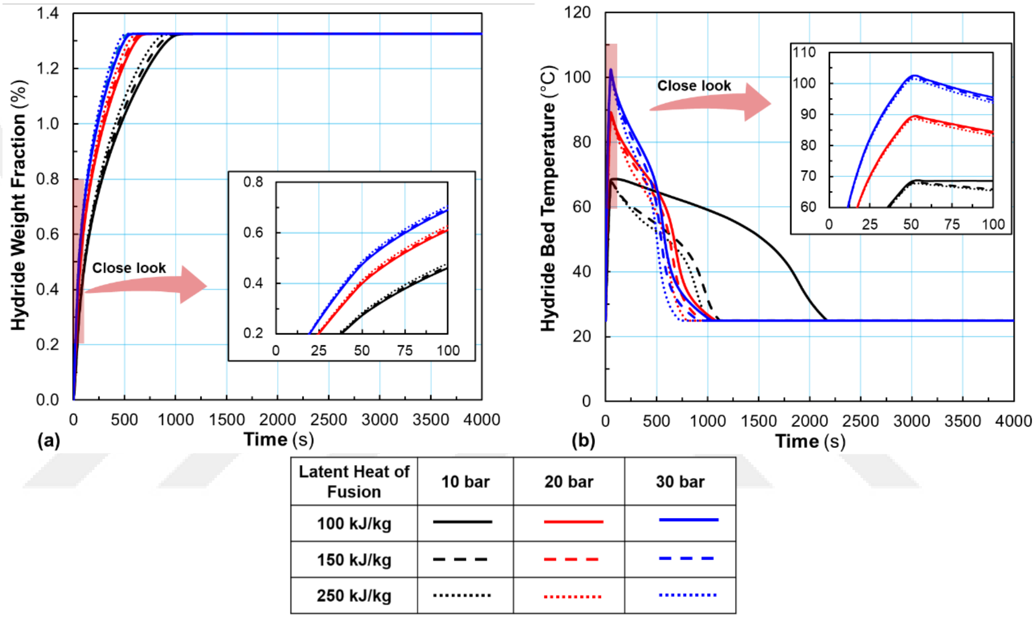

Figure 4.9 Effect of PCM Latent Heat on Time Dependent (a) Weight Fraction (b) Temperature – (T_m = 25 °C, t_{pcm} = 2.5 cm, T_{fluid} = 0 °C, $h_{conv,pipe}$ = 5000 W/m^{2}K)

4.4.3 Influence of Heat Transfer Fluid Temperature Under Different Charging Pressure

In the hybrid thermal management system, the combined parameters of HTF temperature and heat transfer coefficient on storage are presented in Figure 4.10 at two charging pressures. Figure 4.10(a) and (b) show that the storage percentage increases with decreasing heat transfer fluid temperature and increasing convective heat transfer coefficient. At t = 300 seconds, the maximum storage percentages of 73% and 84.75% are observed at 10 and 30 bars charging pressures, respectively. At lower convective heat transfer coefficients, the HTF temperature looks to have little influence on the storage fraction. Beyond a critical convective heat transfer coefficient, i.e., 10000 W/m^{2}K, the storage fraction variations heavily depend on the HTF temperature.

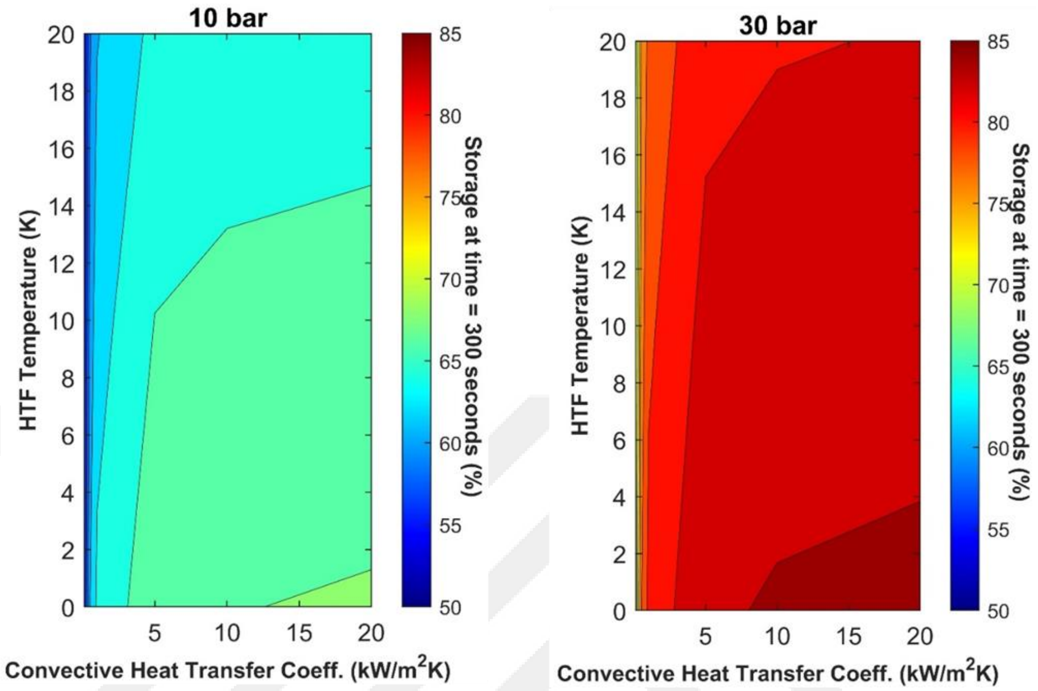

Figure 4.10 The Effect of Heat Transfer Fluid Temperature and Convective Heat Transfer Coefficient on the Storage Percentage at Time is 300 Seconds Under Different Pressures (a) P = 10 (bar) (b) P = 30 (bar)

4.4.4 Local Temperature Distributions

Two *scenarios* are considered to examine the positional temperature variations for two different thermal management systems, i.e., *Scenario*-2 and *Scenario*-3. In Figure 4.11, temperature distributions are comparatively given at t = 120 s, 200 s, and 600 s for selected scenarios. Square markers correspond to the results obtained from Scenario-2. Circles and triangles represent the Scenario-3 with convective heat transfer coefficients of h_{conv} = 5000 W/m^{2}K and h_{conv} = 500 W/m^{2}K, respectively. Results reveal that the hybrid cooling mode, i.e., Scenario-3, keeps the temperatures lower adjacent to the pipe wall, especially at high heat transfer coefficients. Besides, for Scenario-2, the only heat extraction mechanism is the stored energy inside the PCM. In this design, the innermost surface of the reactor is adiabatic, and the temperature variations are uniform adjacent to the pipe. The temperature variations inside the PCM domain look almost identical for t = 120 s and 300 s for each selected scenario. At t =

600 s, the cooling effect from the pipe wall diffuses through the radial direction for Scenario-3 designs, and the mean hydride bed temperatures significantly reduce. The maximum temperature is below 90°C for Scenario-3 with a high convective heat transfer coefficient. The reductions in mean hydride temperatures limit the rise of the PCM temperature, and the spatial temperature variations diverge from each other. The interface temperatures for Scenario-2, Scenario-3 with low convection, and Scenario-3 with high convection are seen to be approximately 50°C, 55°C, and 60°C, respectively (Disli, Cetinkaya, Ezan & Colpan, 2023).

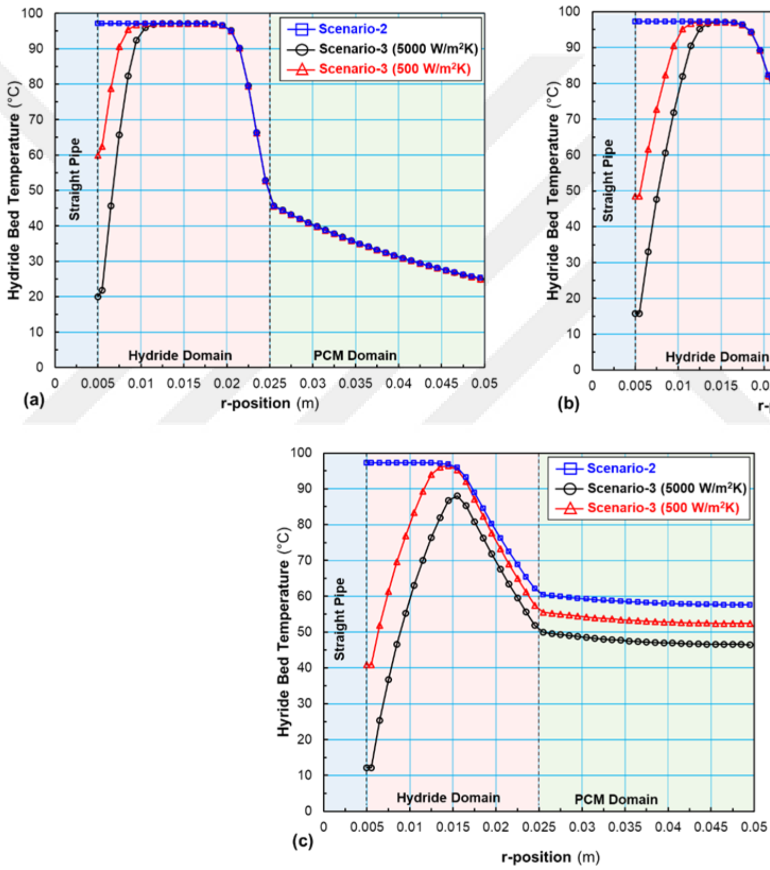

Figure 4.11 Temperature distributions at the mid-height of the MH Tank at *(a) t = 120 s (b) t = 300 s (c) t = 600 s* (T_m = 25°C, t_{pcm} = 2.5 cm, T_{fluid} = 0°C, h_{sf} = 150 kJ/kg)

Figure 4.12 illustrates four positions selected towards the *r*-direction to compare the temporal temperature variations inside PCM and MH tank domains. The time dependent temperatures on the selected notes are presented in Figure 4.13. Regardless of the positions inside the field, the initial trends and peak temperatures overlap in the scenarios chosen. In Scenario-3, the HTF inside the cooling channel is activated when the MH tank temperature exceeds the threshold value, so temperatures tend to diverge from each other beyond the activation. Figure 4.13(a) represents the variations in P1, which is close to the cooling channel. For Scenario 2, the temperature at P1 slightly reduces from 97°C to 82°C. For cases in Scenario-3, the activation of HTF reduces the P1 temperature below 20°C in less than 1000 s and 2000 s for the higher and lower heat transfer coefficients. Reduction in the P1 temperature enhances the heat transfer rate from reactor to the cooling channel. In the centre position of the MH tank, i.e., P2, the peak temperatures are approximately the same as in P1. For Scenario-2, the temperature reduces faster than P1 and oscillates around 82°C. For Scenario-3, temperatures reduce regularly and approach the same steady-state temperature as in P1. P3 and P4 locations correspond to the MH/PCM interface and the mid-point of the PCM, respectively. Since these nodes are close to the exterior surface of the MH tank, the variations are different than P1 and P2. The temperatures increase in time to reach the steady-state temperature of 82°C for Scenario-2 at P3 and P4. For Scenario-3, local temperature maximum can be observed before 1000 s. The maximum lay between 48°C and 55°C. Table 4.4 summarizes temperatures for each position in Figure 4.13. The table also includes temperatures at three selected flow times of 500 s, 1000 s, and 2000 s.

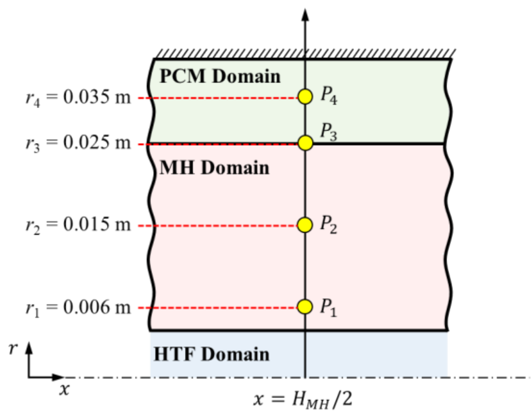

Figure 4.12 Positions of the Selected Inside the Computational Domain

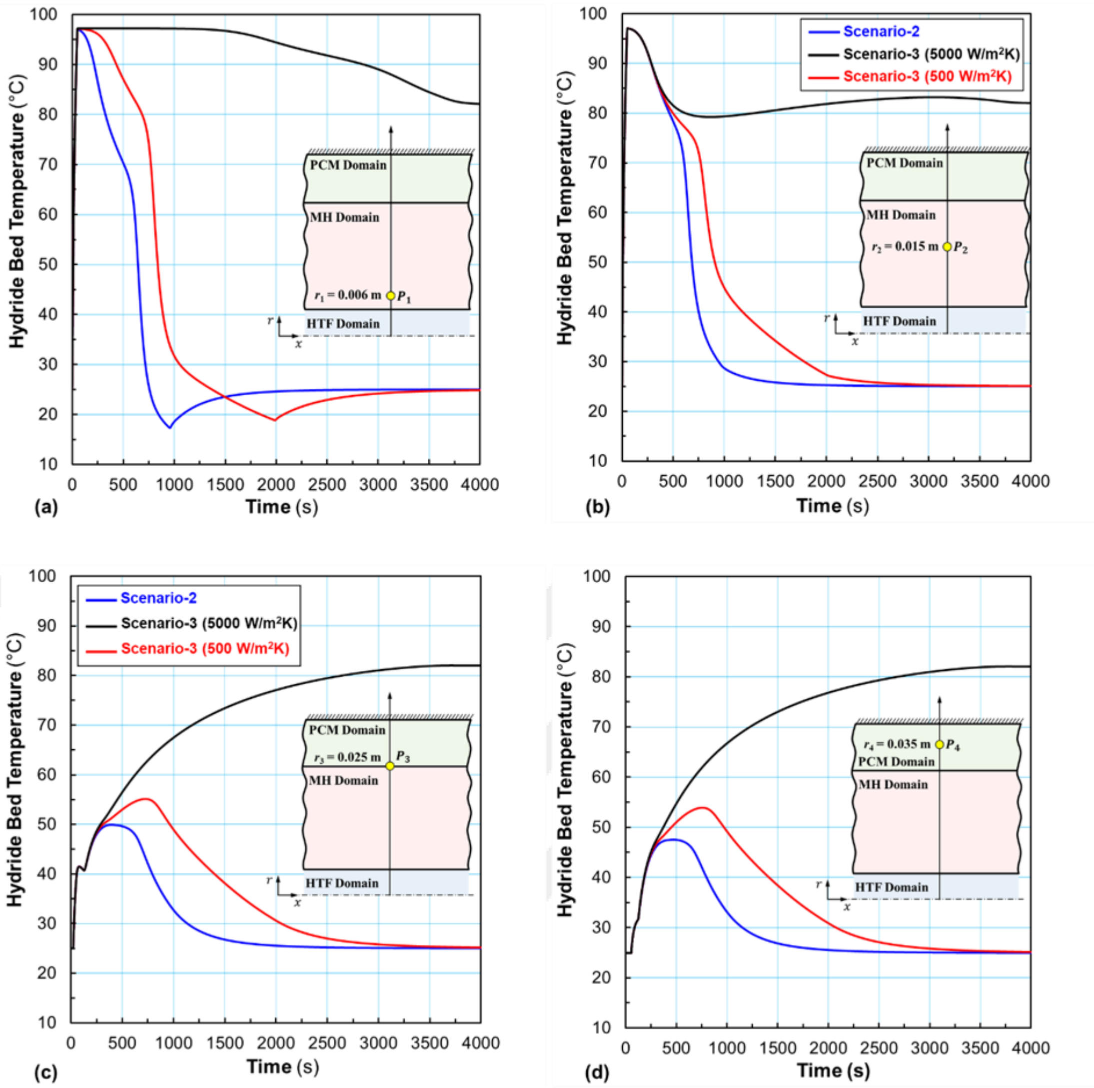

Figure 4.13 Time-wise Variations of Temperatures at (a) P1 (b) P2 (c) P3 (d) P4 for the Selected Scenarios - (T_m = 25°C, t_{pcm} = 2.5 cm, T_{fluid} = 0 °C, $h_{conv,pipe}$ = 5000 W/m2K, h_{sf} = 150 kJ/kg)

Table 4.4 Positional Temperatures in Different Time Periods for Scenario 2 and Scenario 3

Position	**Cases**	**Temperature (°C) t = 500 s**	**Temperature (°C) t = 1000 s**	**Temperature (°C) t = 2000 s**
P1	Scenario-2	97	97	92
	Scenario-3 h_{conv} = 500 W/m^{2}K	88	30	19
	Scenario-3 h_{conv} = 5000 W/m^{2}K	70	21	24
P2	Scenario-2	83	80	82
	Scenario-3 h_{conv} = 500 W/m^{2}K	83	80	82
	Scenario-3 h_{conv} = 5000 W/m^{2}K	82	28	25
P3	Scenario-2	55	68	77
	Scenario-3 h_{conv} = 500 W/m^{2}K	53	49	31
	Scenario-3 h_{conv} = 5000 W/m^{2}K	49	32	25
P4	Scenario-2	53	67	77
	Scenario-3 h_{conv} = 500 W/m^{2}K	51	49	31
	Scenario-3 h_{conv} = 5000 W/m^{2}K	47	32	25

4.5 Comparison of the Effect of Thermal Management Systems on Hydride Bed Temperature and Weight Fraction

In this section, the effects of external forced convection, passive thermal management strategies (PCM) and hybrid thermal management system (PCM and cooling channel) on temperature and storage are presented comparatively.

4.5.1 Influence of PCM Thickness, Cooling Mode Parameter and External Forced Convection Coefficient in Hydride Bed Temperature and Weight Fraction

The effects of PCM thickness and external convection coefficient on MH tank temperature and weight fraction are presented in Figure 4.14. The hydride temperature decreases as the PCM thickness increases in *Scenario*-2 and *Scenario*-3. Considering the time to reach complete charging, S*cenario*-3 with 5 cm of PCM thickness shows the best storage performance with 604 seconds to get the maximum weight ratio. In addition, *Scenario*-1, with an external convection coefficient of 100 W/m^{2}K and Scenario-2 with 2.5 cm of PCM reach complete charging for almost the same duration. However, considering the mean tank temperatures, the active cooling technique looks more promising since in the passive cooling strategy, i.e., PCM incorporation, the tank temperature is as much as 80°C. Increasing the external convection coefficient from 100 W/m^{2}K to 500 W/m^{2}K in *Scenario*-1, the time for complete charging reduces by almost 1200 s.

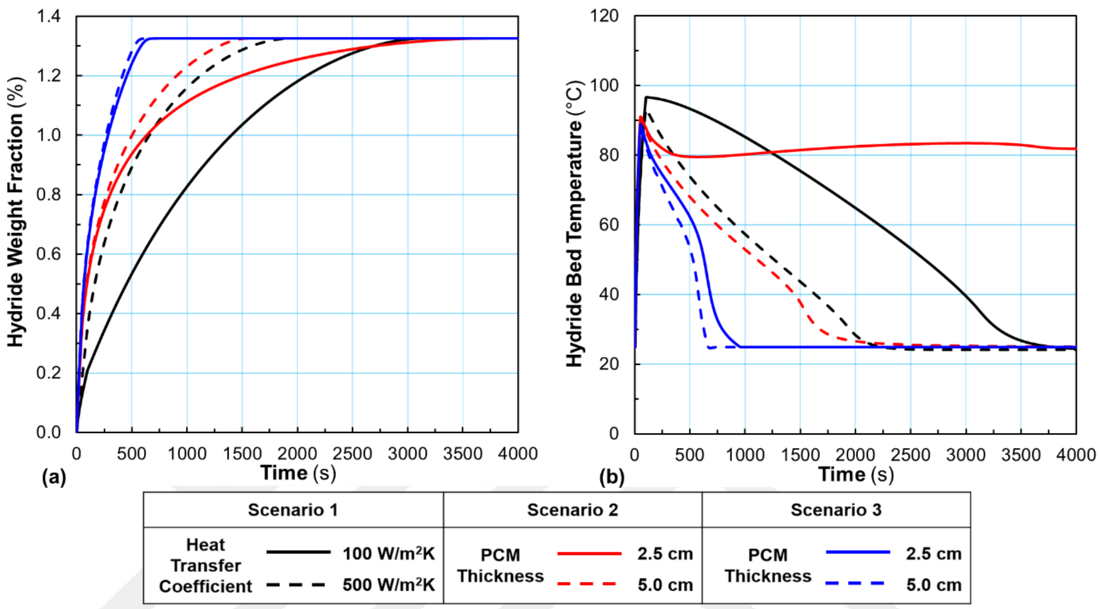

Figure 4.14 The Effect of 3 Different Scenario Parameters (a) Weight Fraction (b) Bed Temperature

4.5.2 Influences of Latent Heat of PCM and External Convective Heat Transfer Coefficient

Figure 4.15 illustrates the impact of latent heat and external convection coefficient on weight fraction and hydride bed temperature. In Figure 4.15(a), Scenario-3 exhibits the highest weight fraction of 250 kJ/kg fusion heat at 603 seconds, whereas the maximum weight fraction time for 150 kJ/kg latent heat value is 612 seconds. It was observed that an increase in latent heat does not significantly affect weight fraction beyond a specific limit. Additionally, increasing the external convection coefficient reduces the time to reach the maximum weight fraction. When Scenario-1 with an external convection coefficient (500 W/m^{2}K) was selected, and it approached Scenario-2, offering passive thermal management.

According to Figure 4.15(b), Scenario-3 exhibits the minimum time drop to 25°C, and a difference of 108 seconds was observed with an enhance in latent heat. At 100 kJ/kg of latent heat, Scenario-2 cools the hydride bed temperature to 51°C, while the hydride bed temperature drops to 33°C for latent heat is 250 kJ/kg. In an inactive cooling channel, an increase in latent heat has a significant impact compared to Scenario-3. On the other hand, with the increase of the external convection coefficient from 100 W/m^{2}K to 500 W/m^{2}K, the time to attain the external temperature of the hydride bed decreased by approximately 1500 seconds. It is strongly observed that when an appropriate value is selected for the external convection coefficient, it provides a cooling performance greater than the cooling performance of PCM (Scenario-2).

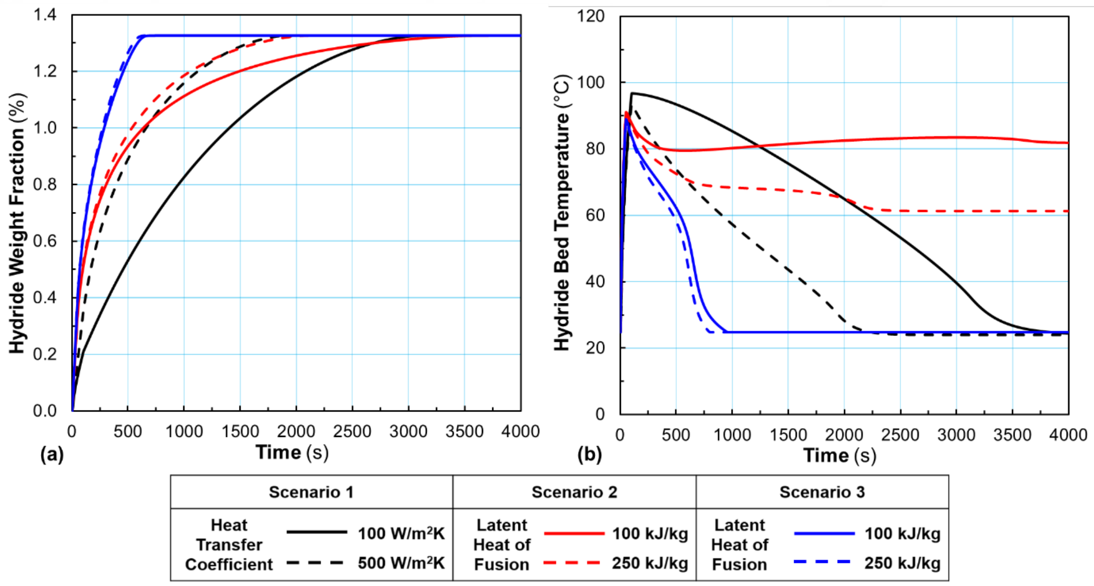

Figure 4.15 The Effect of Latent Heat and External Convection Coefficient on Weight Fraction and Temperature for 3 Different Scenarios

4.5.3 Overall Assessments on Absorption Process Under Different Charging Pressure

Figure 4.16 presents the full storage time and weight fraction at t = 300 seconds for three thermal management systems and three different charging pressures of the $LaNi_5$-based hydride bed. The hybrid thermal management system outperforms the other scenarios regarding a reduced time to achieve complete storage for all three charging pressures. The minimum time for complete storage is observed at 610 seconds in the case with 30 bar of charging pressure and a hybrid thermal management system. Considering the constant parameters, the advantage of the convection coefficient chosen for Scenario-1 is significantly higher than the cooling provided by the PCM thickness and latent heat determined for Scenario-2. The constant parameters in the analysis are given in Table 5 for each scenario.

Weight fractions at t=300 seconds were calculated for three different charging pressures. The hybrid thermal management system has the highest weight ratio of all charge pressures. For 30 bar charge pressure and scenario 3, the weight ratio at 300 seconds is 1.11%. In contrast scenario-2 has the lowest weight ratio for all charging pressures. The parametric analysis shows that the convection coefficient used in scenario-1 is a more effective parameter in providing a better thermal management system compared to the PCM thickness and latent heat of fusion.

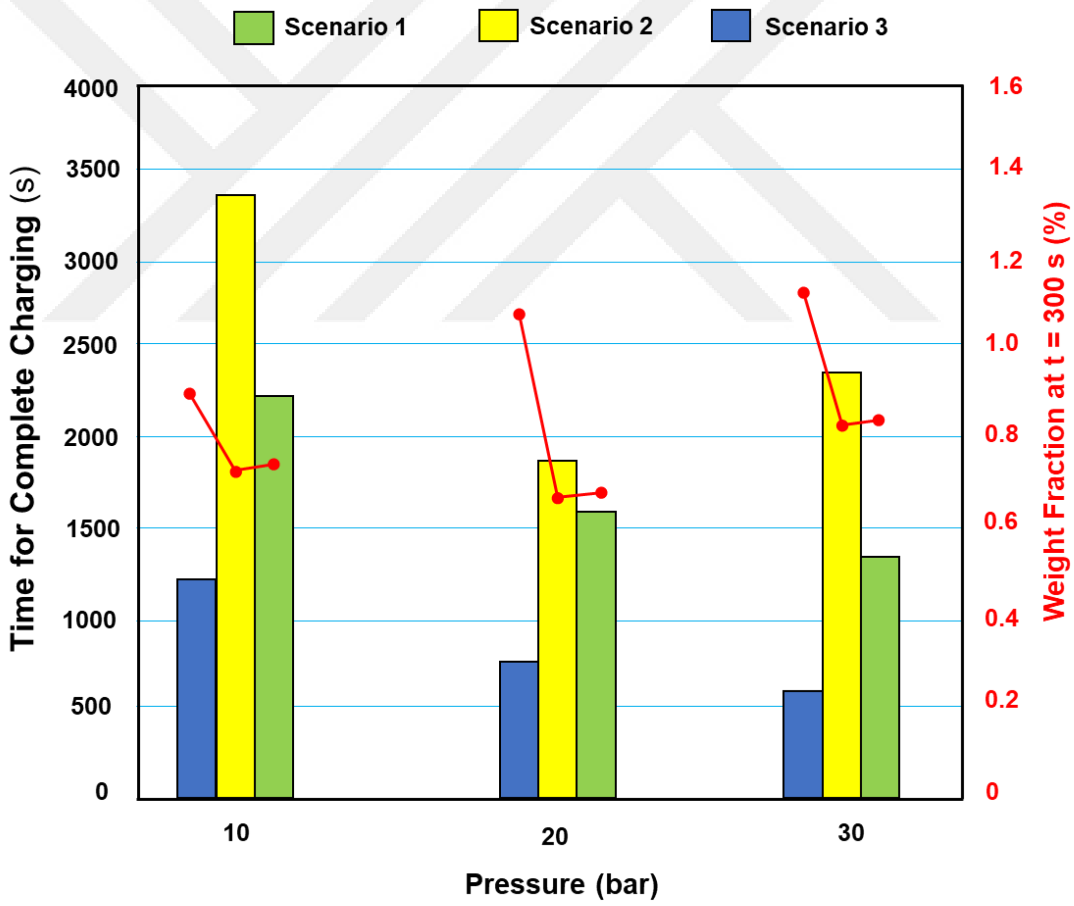

Figure 4.16 Complete Charging Time and Weight Fraction at $t = 300\ S$ for Three Different Scenarios under Different Charging Pressures

CHAPTER FIVE
CONCLUSIONS

In this thesis, a 2D axisymmetric model has been developed using MATLAB software to predict the storage criteria and hydride bed temperature in a $LaNi_5$ based metal hydride reactor. After the model was validated with the literature, the effects of different thermal management systems on the hydride bed were investigated. Paraffin was chosen for $LaNi_5$ as the PCM. The storage performances of the system for the external forced convection, phase change material and cooling channel-phase change material scenarios have been extensively investigated. In scenario-1, forced convection is applied to the lateral surfaces as a thermal management system. In scenario-2, PCM is wrapped around the tank to cool the reactor. In scenario-3, both the PCM and the HTF passing through the central pipe provide the thermal management system of the hydride reactor. According to present study, following conclusions are obtained,

- The increase in the filling percentage is strongly connected on the increase in the external temperature and external convection coefficient.
- In comparison between Scenarios 2 and 3, it can be observed that the weight fraction decreases in Scenario-2 with the increase of pressure from 20 to 30 bar. In Scenario-3, this reduction in weight fraction was reversed by the effect of heat transfer fluid using hybrid thermal management.
- At the positional temperature distribution, internal heat load increase in the hydride domain is minimized by implementation a hybrid thermal management system with a high convection coefficient inside the cooling channel.
- Considering Scenarios 1 and 2, it can be seen that it is a lot of advantageous in the case of a high heat transfer coefficient than in the case of low PCM thickness. In this case, if the PCM thickness is not selected in appropriate sizes, situations with a high heat convection coefficient can be preferred for thermal management.

- Compared to Scenarios-1 and 2, the effect of active thermal management in Scenario 3 can be observed by minimizing the hydride temperature and providing faster storage.
- The minimum time for complete storage can be observed as 550 seconds in Scenario-3. For the feasibility of the parameters, the convection coefficient selected for Scenario-1 performed better than the PCM thickness and latent heat determined for Scenario-2 in terms of cooling. Consequently, for fast and complete charging, Scenario-3 is effective, and the operating parameters should be chosen appropriately.

In response to the increasing demand for hydrogen, the step-up in the use of hydrogen systems (e.g., fuel cell vehicles) indicates that hydrogen storage will also occupy a vital topic in the future. The chemical structure of MH requires thermal management to obtain hydrogen at the desired flow rate. This study was executed to investigate the effect of passive and active thermal management on storage performance and aims to guide future studies on this subject. Considering the results, it is important to correctly determine and analyze the boundary conditions to choose the proper thermal management according to the situation in which the MH tank will be used.

More comprehensive parametric analyzes can be listed on topics that can lead to future studies by applying the thermal management systems within the scope of the thesis. Fuel cell, hydrogen compressor, hydrogen electrolyzer and metal hydride tank can be considered together, the effect of the thermal management strategies on the integrated system can be examined and a comprehensive design space can be created.

REFERENCES

Afzal, M., Mane, R., & Sharma, P. (2017). Heat transfer techniques in metal hydride hydrogen storage: A review. *International Journal of Hydrogen Energy*, *42*(52), 30661–30682.

Aldas, K., Mat, M. D., & Kaplan, Y. (2002). A three-dimensional mathematical model for absorption in a metal hydride bed. *International Journal of Hydrogen Energy*, *27*(10), 1049–1056.

Alqahtani, T., Mellouli, S., Bamasag, A., Askri, F., & Phelan, P. E. (2020). Thermal performance analysis of a metal hydride reactor encircled by a phase change material sandwich bed. *International Journal of Hydrogen Energy*, *45*(43), 23076–23092.

Askri, F. (2003). Study of two-dimensional and dynamic heat and mass transfer in a metal–hydrogen reactor. *International Journal of Hydrogen Energy*, *28*(5), 537–557.

Askri, F. (2004). Prediction of transient heat and mass transfer in a closed metal–hydrogen reactor. *International Journal of Hydrogen Energy*, *29*(2), 195–208.

Askri, F., Bensalah, M., Jemni, A., & Ben Nasrallah, S. (2009). Optimization of hydrogen storage in metal-hydride tanks. *International Journal of Hydrogen Energy*, *34*(2), 897–905.

Bai, X.-S., Yang, W.-W., Tang, X.-Y., Dai, Z.-Q., & Yang, F.-S. (2022). Parametric optimization of coupled fin-metal foam metal hydride bed towards enhanced hydrogen absorption performance of metal hydride hydrogen storage device. *Energy*, *243*, 123044.

Bao, Z., Yang, F., Wu, Z., Cao, X., & Zhang, Z. (2013). Simulation studies on heat and mass transfer in high-temperature magnesium hydride reactors. *Applied Energy*, *112*, 1181–1189.

Barthelemy, H., Weber, M., & Barbier, F. (2017). Hydrogen storage: Recent improvements and industrial perspectives. *International Journal of Hydrogen Energy*, *42*(11), 7254–7262.

Borzenko, V., & Eronin, A. (2016). The use of air as heating agent in hydrogen metal hydride storage coupled with PEM fuel cell. *International Journal of Hydrogen Energy*, *41*(48), 23120–23124.

Busqué, R., Torres, R., Grau, J., Roda, V., & Husar, A. (2018). Mathematical modeling, numerical simulation and experimental comparison of the desorption process in a metal hydride hydrogen storage system. *International Journal of Hydrogen Energy*, *43*(35), 16929–16940.

Cengel, Y., & Ghajar, A. (2015). *Heat and Mass Transfer* (Fifth Edit). McGraw-Hill Education. https://www.ptonline.com/articles/how-to-get-better-mfi-results

Cetinkaya, S. A., Disli, T., Soyturk, G., Kizilkan, O., & Colpan, C. O. (2022). A Review on Thermal Coupling of Metal Hydride Storage Tanks with Fuel Cells and Electrolyzers. *Energies*, *16*(1), 341.

Chung, C. A., Chen, Y.-Z., Chen, Y.-P., & Chang, M.-S. (2015). CFD investigation on performance enhancement of metal hydride hydrogen storage vessels using heat pipes. *Applied Thermal Engineering*, *91*, 434–446.

Dincer, I. (2020). Covid-19 coronavirus: Closing carbon age, but opening hydrogen age. *International Journal of Energy Research*, *44*(8), 6093–6097.

Dincer, I., & Ezan, M. A. (2018). *Heat Storage: A Unique Solution For Energy Systems*. Springer International Publishing.

El Mghari, H., Huot, J., Tong, L., & Xiao, J. (2020). Selection of phase change materials, metal foams and geometries for improving metal hydride performance. *International Journal of Hydrogen Energy*, *45*(29), 14922–14939.

El Mghari, H., Huot, J., & Xiao, J. (2019). Analysis of hydrogen storage performance of metal hydride reactor with phase change materials. *International Journal of Hydrogen Energy*, *44*(54), 28893–28908.

Facci, A. L., Lauricella, M., Succi, S., Villani, V., & Falcucci, G. (2021). Optimized Modeling and Design of a PCM-Enhanced H2 Storage. *Energies*, *14*(6), 1554.

Gupta, S., & Sharma, V. K. (2021). Design and analysis of metal hydride reactor embedded with internal copper fins and external water cooling. *International Journal of Energy Research*, *45*(2), 1836–1856. https://doi.org/10.1002/er.5859

Hariyadi, A., Suwarno, S., Denys, R. V., von Colbe, J. B., Sætre, T. O., & Yartys, V. (2022). Modeling of the hydrogen sorption kinetics in an AB2 laves type metal hydride alloy. *Journal of Alloys and Compounds*, *893*, 162135.

Hassan, I. A., Mohammed, R. H., Ramadan, H. S., Saleh, M. A., Cuevas, F., & Hissel, D. (2023). Performance evaluation of a novel concentric metal hydride reactor assisted with phase change material. *Applied Thermal Engineering*, *224*, 120065.

Jemni, A. (1995). Study of two-dimensional heat and mass transfer during absorption in a metal-hydrogen reactor. *International Journal of Hydrogen Energy*, *20*(1), 43–52. https://doi.org/10.1016/0360-3199(93)E0007-8

Karmakar, A., Mallik, A., Gupta, N., & Sharma, P. (2021). Studies on 10kg alloy mass metal hydride based reactor for hydrogen storage. *International Journal of Hydrogen Energy*, *46*(7), 5495–5506.

Kumar, A., Raju, N. N., Muthukumar, P., & Selvan, P. V. (2019). Experimental studies on industrial scale metal hydride based hydrogen storage system with embedded cooling tubes. *International Journal of Hydrogen Energy*, *44*(26), 13549–13560.

Madaria, Y., & Anil Kumar, E. (2016). Effect of heat transfer enhancement on the performance of metal hydride based hydrogen compressor. *International Journal of Hydrogen Energy*, *41*(6), 3961–3973.

Mellouli, S., Askri, F., Dhaou, H., Jemni, A., & Ben Nasrallah, S. (2010). Numerical simulation of heat and mass transfer in metal hydride hydrogen storage tanks for fuel cell vehicles. *International Journal of Hydrogen Energy*, *35*(4), 1693–1705.

Miled, A., Mellouli, S., Ben Maad, H., & Askri, F. (2017). Improvement of the performance of metal hydride pump by using phase change heat exchanger. *International Journal of Hydrogen Energy*, *42*(42), 26343–26361.

Mohamed, F. A. (2019). *Experimental And Numerical Investigations of Effect of A Heat Pipe in the Metal Hydride Tank for the Hydriding Process Energy Systems Engıneering*. Master Science of Thesis.

Møller, K. T., Jensen, T. R., Akiba, E., & Li, H. (2017). Hydrogen - A sustainable energy carrier. *Progress in Natural Science: Materials International*, *27*(1), 34–40.

Montenegro, A. R., Sanjuan, M., & Carmona, M. (2019). Energy Storage Development Using Hydrogen and Its Potential Application in Colombia. *International Journal of Energy Economics and Policy*, *9*(6), 254–268.

Muthukumar, P., Kumar, A., Raju, N. N., Malleswararao, K., & Rahman, M. M. (2018). A critical review on design aspects and developmental status of metal hydride based thermal machines. *International Journal of Hydrogen Energy*, *43*(37), 17753–17779.

Nakagawa, T. (2000). Numerical analysis of heat and mass transfer characteristics in the metal hydride bed. *International Journal of Hydrogen Energy*, *25*(4), 339–350.

Nasrallah, S. (1997). Heat and mass transfer models in metal-hydrogen reactor. *International Journal of Hydrogen Energy*, *22*(1), 67–76.

Nitta, I., Himanen, O., & Mikkola, M. (2008). Thermal Conductivity and Contact Resistance of Compressed Gas Diffusion Layer of PEM Fuel Cell. *Fuel Cells*, *8*(2), 111–119.

Rabienataj Darzi, A. A., Hassanzadeh Afrouzi, H., Moshfegh, A., & Farhadi, M. (2016). Absorption and desorption of hydrogen in long metal hydride tank equipped with phase change material jacket. *International Journal of Hydrogen Energy*, *41*(22), 9595–9610.

Sandrock, G. (1999). A panoramic overview of hydrogen storage alloys from a gas reaction point of view. *Journal of Alloys and Compounds*, *293–295*, 877–888.

Suda, S., Komazaki, Y., & Kobayashi, N. (1983). Effective thermal conductivity of metal hydride beds. *Journal of the Less Common Metals*, *89*(2), 317–324.

Tong, L., Xiao, J., Bénard, P., & Chahine, R. (2019). Thermal management of metal hydride hydrogen storage reservoir using phase change materials. *International Journal of Hydrogen Energy*, *44*(38), 21055–21066.

Tong, L., Xiao, J., Yang, T., Bénard, P., & Chahine, R. (2019). Complete and reduced models for metal hydride reactor with coiled-tube heat exchanger. *International Journal of Hydrogen Energy*, *44*(30), 15907–15916.

Ye, Y., Lu, J., Ding, J., Wang, W., & Yan, J. (2020). Numerical simulation on the storage performance of a phase change materials based metal hydride hydrogen storage tank. *Applied Energy*, *278*, 115682.

Yilmaz, G., Sadvakasova, A. K., Kossalbayev, B. D., Bauenova, M. O., Zharmukhamedov, S. K., Ziyayeva, G. K., Zaletova, D. E., Alharby, H. F., & Allakhverdiev, S. I. (2023). Hydrogen energy development in Turkey: Challenges and opportunities. *International Journal of Hydrogen Energy*.

Zhou, L. (2005). Progress and problems in hydrogen storage methods. *Renewable and Sustainable Energy Reviews*, *9*(4), 395–408.

Züttel, A. (2004). Hydrogen storage methods. *Naturwissenschaften*, *91*(4), 157–172.

APPENDICES

Appendix – 1: Nomenclature

A, B	Plateu pressure coefficients [-], [K^{-1}]
C	Volumetric heat capacity [J m^{-3} K^{-1}]
C_a	Reaction constant in absorption process [s^{-1}]
c_p	Specific heat capacity [J kg^{-1} K^{-1}]
E_a	The activation energy in the absorption process [J mol^{-1}]
H	Reaction enthalpy [J kg^{-1}]
h	Convective heat transfer coefficient [W m^{-2} K^{-1}]
h_{sf}	Latent heat of fusion [J kg^{-1}]
k	Thermal conductivity [W $m^{-1}$$K^{-1}$]
$\dot{m}'''$	Volumetric mass flow rate [kg m^{-3} s^{-1}]
P	Pressure [bar]
R	Universal gas constant [J mol^{-1} K^{-1}]
S	Source term in energy equation [W m^{-3}]
T	Temperature [K]
t	Time [s]
x, r	Axial and radial coordinates [m]

Greek Letters

ρ	Density [kg m^{-3}]
ε	Porosity [-]
ΔH^0	Enthalpy of formation [kJ kg^{-1}]
δT_m	The mushy phase temperature range [K]

Subscripts

eff	Effective
en	Enhance

eq	Equivalent
g	Gas
lim	Limit
lp	Liquid phase
m	Melting
mp	Mushy phase
ref	Reference
s	Solid
sp	Solid phase
ss	Saturated state

Abbreviations

CFD	Computational Fluid Dynamics
HTF	Heat Transfer Fluid
MH	Metal Hydride Tank
PCM	Phase Change Material